Università Cattolica del Sacro Cuore

Sede di Brescia

Facoltà di Scienze Matematiche, Fisiche e Naturali

Corso di Laurea in Fisica

Tesi di Laurea

Temporal Characterization of Short Laser Pulses in Microscopy

Relatore:

Dott. Francesco Banfi

Correlatore:

Dott. Gabriele Ferrini

Laureando: **Fabio Medeghini**

mat. 4109071

Anno Accademico 2013/2014

Contents

1 Introduction **1**
- 1.1 Overview . . . 1
- 1.2 Outline . . . 2

2 Setup for time-resolved optical microscopy measurements **3**
- 2.1 Pump & probe technique [1] [2] . . . 3
- 2.2 ASOPS technique [1] . . . 5
  - 2.2.1 Working principle of ASOPS . . . 5
- 2.3 Setup idealization . . . 7

3 Temporal characterization of an ultrashort laser pulse **9**
- 3.1 Temporal characterization [13] . . . 9
- 3.2 Experimental apparatus [14] [15] . . . 11
- 3.3 FROG phase-retrieval algorithm [14] [15] [13] . . . 14
- 3.4 FROG geometries [13] [16] [17] . . . 18
  - 3.4.1 PG FROG . . . 18
  - 3.4.2 SD FROG . . . 20
  - 3.4.3 TG FROG . . . 21
  - 3.4.4 SHG FROG . . . 23
  - 3.4.5 THG FROG . . . 24
  - 3.4.6 XFROG . . . 26
  - 3.4.7 Summary . . . 29

4 SHG FROG in microscopy **31**
- 4.1 Collinear SHG FROG [19] . . . 31
- 4.2 Collinear SHG FROG for pump characterization . . . 33
- 4.3 Numerical simulations for SHG FROG [18] . . . 33
  - 4.3.1 Gaussian profile, constant phase . . . 35
  - 4.3.2 Gaussian profile, square phase . . . 37
  - 4.3.3 Gaussian profile, cubic phase . . . 39
  - 4.3.4 Double Gaussian profile, constant phase . . . 40

5 SFG XROG in supercontinuum **45**
5.1 Collinear SFG XFROG [17] [20] [21] 45
5.2 SFG XFROG for SC probe characterization 48

6 Prospectives and conclusions **51**

7 Acronimi **53**

Chapter 1

Introduction

1.1 Overview

The energy carriers transfers in nanosystems occurs on temporal scales ranging from a few picoseconds to about tens nanoseconds depending on the system's size and composition and on sub-micrometric spatial scales. One can follow the thermomechanical dynamics on these scales using a pump & probe optical technique coupled to an appropriate tailored microscopy system. This technique requires the spatial and temporal characterization of both the pump and probe pulses at the foci of the microscope objective. The spatial characterization has already been discussed in my previous thesis work [1]. The temporal characterization will be the topic of this thesis work and will be dealt with exploiting the so called FROG technique. FROG is the acronym for *frequency-resolved optical gating*, a technique for the characterization of femtosecond pulses. The FROG method requires a simple experimental system, based on an instantaneous non-linear optical effect. From a single arbitrary laser pulse, that is split into two, an experimental FROG trace is obtained, encompassing both frequency and temporal informations on the pulse. The FROG trace allows to retrieve the intensity and phase evolution of the input pulse without significant ambiguities. This retrieval can be accomplished with the implementation of an iterative algorithm based on the Fourier transform. Operating with a collinear geometry, it is possible to exploit the FROG in the ultrashort pulses characterization at the focal region of an objective with elevated numerical aperture. In case the specific pump & probe technique uses probe pulses with a supercontinuum spectrum, generated by a photonic crystal fiber, it is convenient to use the XFROG technique for the temporal characterization of the probe pulses. The XFROG, *cross-correlation frequency-resolved optical gating*, indicates a variant of the FROG that uses the probe and the pump pulse (rather than two replicas of the probe pulse) to produce the experimental XFROG trace. This variant can be very sensible, intuitive, and it can be applied to several spectral regions.

1.2 Outline

The aim of this thesis work is the temporal characterization of the pulses in a pump & probe technique at the focal region of the microscope objective, where the pump pulses are monochromatic laser pulses, while the probe pulses are supercontinuum pulses.

Chapter two consist in a description of the pump & probe and ASOPS techniques. Follow the idealization of a reference setup based on these techniques.

Chapter three deal with the FROG technique. At the beginning is explained what it is meant for temporal characterization of ultrashort pulses. The FROG technique is then illustrated through the description of the experimental apparatus and phase-retrieval algorithm. Well-known FROG geometries are briefly presented, with respective advantages and disadvantages.

Chapter four focuses on the use of the collinear second-harmonic-generation (SHG) FROG in microscopy. Here is studied the feasibility of an application of this FROG geometry to the reference setup for the characterization of the pump pulse. To the purpose of testing the FROG algorithm in the SHG case, some simple numerical simulation were made.

Chapter five is about the use of the collinear sum-frequency-generation (SFG) XFROG in microscopy. Here is analyzed the feasibility of an application of this XFROG geometry to the reference setup for the characterization of the ultrabroad supercontinuum (SC) probe pulse.

Chapter 2

Setup for time-resolved optical microscopy measurements

In this Chapter is described the idealization of an experimental setup for time-resolved optical microscopy measurements on nanostructured samples. Such a setup is based on the pump & probe technique which allows to follow the temporal dynamic of a sample. Moreover, it exploits the ASOPS technique that permits a calibration of the delay between pump & probe pulses in an electronic way, instead of mechanical. Since we are interested in a setup designed to work on nanoscopical samples, it is required the use of a microscope system able to focuses the pump & probe pulses on the sample. Since the interaction between laser pulses and samples happens to be at the focus level, it is important to characterized the pulses in this point.

2.1 Pump & probe technique [1] [2]

The use of ultra-short pulsed laser beams allows to analyze physical phenomena with a temporal resolution of the femtosecond by the use of pulses with high amplitudes, but tiny average energies, namely with no risk of ruin the samples. By means of a Titanium-Sapphire oscillator, it is possible to obtain pulses at a wavelength of 800 nm characterized by a temporal length below the $4 - 5$ fs.

Thanks to this kind of technology, if one has to handle samples composed by molecules or atoms that absorb the incident radiation, it is possible to realize a pump & probe experiment. The majority of the ultra-fast spectroscopy experiments are based on the pump & probe technique. Typically the pump beam is much more intense than the probe one (in such a way the pump is used to exciting the sample, while the probe yields a negligible perturbation on it) and the two beams can be at different wavelengths. The pump pulse induces a process on the sample that can be, for instance, a chemical process or an electronic excitation. Once excited, the sample will relax towards its non-perturbed state in a characteristic time (much longer than the pulse length) and then it will be excited again through the following pulse. The probe pulse, incoming with a known delay with respect to the pump, will show a distortion dependent on the

change experienced from the sample. The power of this technique lies in the fact that the delay of the probe pulse in respect to the pump one can be variated. In this way, one can follow the entire excitation and relaxation dynamics of the sample. Indeed, the probe will 'feel' an intense distortion when it arrives on the sample simultaneously to the pump, while it will remain substantially unchanged when its delay is such that the sample is already relaxed. Once one get the excitation versus delay graphic, it is possible to go back to the physical properties of the sample.
What it is measured through this technique is the variation of the relative transmission (or relative reflectivity) of the sample material. Inducing a perturbation in the electronic structure of the material, its optical properties will change. The perturbation is produced through a pump pulse, while the transmission variation is examined with the probe pulses. If the probe pulses arrive on the sample with temporal delays increasing in respect to the pump ones, then it will be possible to follow the relaxing dynamics of the sample from its excited state to the unperturbed one. A typical pump & probe measurement yields a curve similar to the one shown in Fig. (2.1).

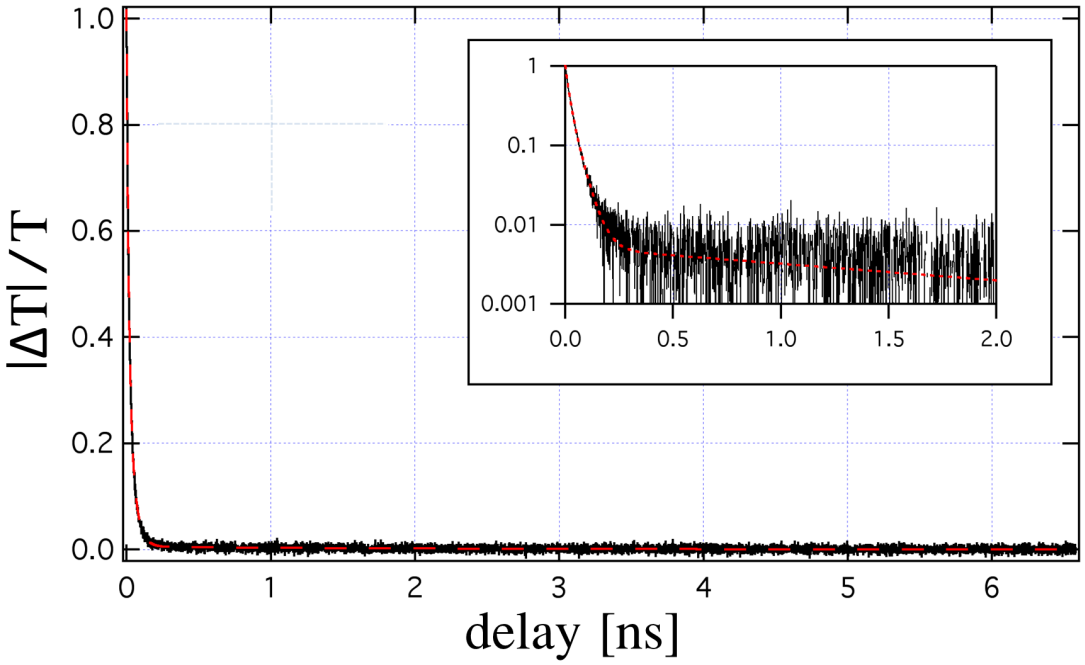

Figure 2.1: Variation of the relative transmission in function of the delay between pump and probe. Inset: same curve reported in logarithmic scale where is pointed out the delay in the range $0 - 2\,\text{ns}$. The maximum occurs when the probe pulse is simultaneous to the pump one; as the delay increases, the probe 'see' the sample returning to its unperturbed state.

2.2 ASOPS technique [1]

A setup for time-resolved measurements on nanostructured samples must be able to follow the entire relaxing dynamics of the samples, which involves times from 100 ps a 10 ns. The traditional technique used to examine those temporal range is the pump & probe technique based on a mechanical delay line. The delay line leads the pump pulse along an optical arm which increase its path length of ones choosing. In this way the two pulses (pump and probe) arrived on the sample with a defined delay between them. Controlling the length difference between the pump and the probe path, one can supervise the mutual delay. Varying this delay each time, it is possible to follow the relaxing dynamics of the sample. This technique allows to obtain time-resolved measurements with an excellent temporal resolution. Anyway it exhibits remarkable problems when the temporal range to examine exceed the hundreds of ps. The problems are the following [3]:

- A long delay line makes the conservation of the spatial coincidence between pump and probe beams harder. For instance, imagine an experiment where the diameters of the pump and probe beams are 60 and 40 μm respectively, and that where we want to follow a temporal dynamics of 10 ns. In this case the two beams should be kept in coincidence with a spatial tolerance of about 5 μm, varying the optical path of 3 m.

- The data capturing is very slow because every time one need to move the translation stage to change the optical path. A slow data capture introduces problems in terms of stability of the experimental line (thermal laser fluctuations, optical fluctuations, temperature instability in cryogenic measurements, etc.).

- The problem listed above are intensified when the technique is applied in microscopy. In such a case, the acceptance conditions on the spatial misalliance result to be even tighter.

These problems can be fixed using a pump & probe technique based on the Asynchronous Optical Sampling (ASOPS) Technique which does not involve the movement of mechanical parts (no delay line). From here on with the term ASOPS will be indicated the laser system and the electronics linked that allow an asynchronous optical sampling.

2.2.1 Working principle of ASOPS

The ASOPS considered in this work is composed by two lasers with wavelength of 780 nm and 1560 nm. These lasers are pulsed and the pulse length is about 150 fs. The electronics allows to have a repetition-rate $f_r = 100$ MHz for the pump laser and of 100 MHz plus a small detuning value $f_r + \Delta f$ for the probe laser.

Defying the repetition-rate frequencies of the two lasers as $f_{pump} = f_r$ and $f_{probe} =$

$f_r + \Delta f$, the temporal delay Δt between them will be

$$\Delta t = \left| \frac{1}{f_{pump}} - \frac{1}{f_{probe}} \right| = \frac{\Delta f}{f_{pump} \cdot f_{probe}}. \tag{2.1}$$

Assuming the frequency difference Δf to be very small and developing Eq. (2.1) in power series, one obtain

$$\Delta t \approx \frac{\Delta f}{f_r^2}. \tag{2.2}$$

For every pulse the probe beam collects a delay Δt until to find itself again in coincidence with a pump pulse, after a time interval of $1/\Delta f$. The working principle of the detuning is schematically reported in Fig. (2.2).

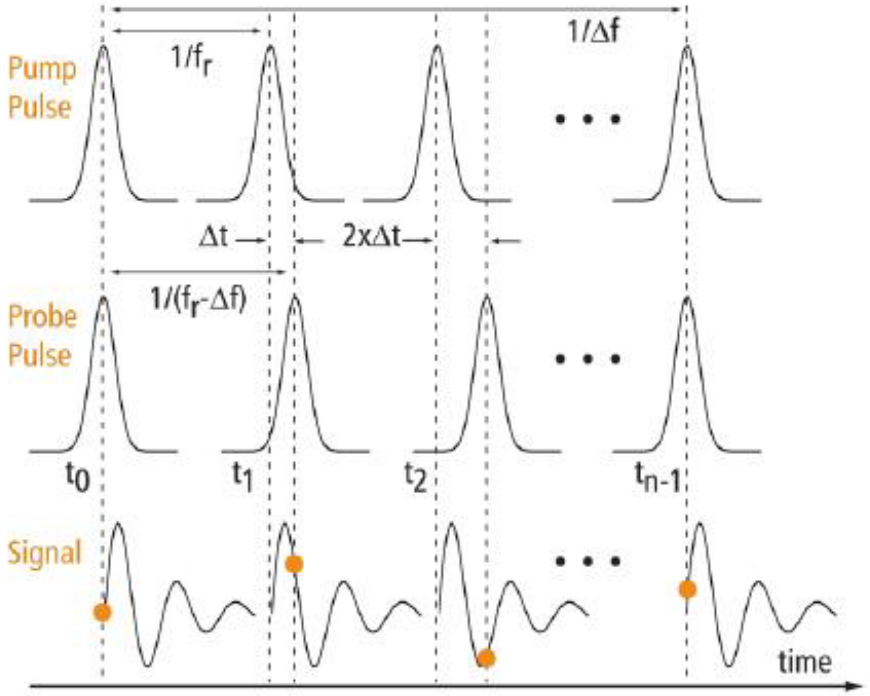

Figure 2.2: Operating principle of the ASOPS technique. The image has been taken from the technical manual for the use of the ASOPS [4]. In figure is shown the mutual temporal delay between the pump and the probe pulse. Because of the detuning Δf between the pulses of the two lasers, a progressive temporal delay between them is generated, and this allows to measure the thermal relaxing dynamics of the sample at different temporal delays.

The electronic management of the delay between the two laser pulses avoids the problems which characterized the traditional pump & probe method. Indeed, the generation of temporal delay without a mechanical translation stage avoids the problems relating to the spatial coincidence of the two laser beams. With the traditional technique, the

time required to investigate an interval of 10 ns with a temporal resolution of 150 fs is on the order of the hour, while with the use of the ASOPS the same measurement is settled in 1 ms [1]. As concern the temporal range, with the traditional technique typically one has an interval on the order of the ns [3, 5, 6, 7, 8] o inferiore [9, 10, 11, 12], while using the ASOPS the temporal range is increased of one order of magnitude, that is 10 ns.

2.3 Setup idealization

The experimental setup that we will use as a reference in this work is schematically reported in Fig. (2.3). This setup is conceived for time-resolved optical microscopy measurements on nanostructured samples. These measurements are achieved through the pump & probe technique based on the ASOPS technique (no mechanical delay line). Specifically, the pump beam work @ 1560 nm, while the probe, that initially is @ 780 nm, its used for broadband supercontinuum (SC) generation through a photonic-crystal fiber. Therefore the pump and the probe spectra are 'monochromatic' and 'polichromatic' respectively. This allows to investigate the sample response at various wavelength. A beam splitter divides the SC probe beam in a SC reference beam, which is led towards a delay line, and in a SC probe beam, that proceeds to the sample in spatial coincidence with the pump beam. Since we want to study the dynamics of nanostructured samples, the pump and SC probe beams must be focus on the sample by the means of a microscope system. The output SC probe beam is then compared frequency-by-frequency with the SC reference beam through two monochromators and a differential photodiode. Here the delay line of the SC reference beam must be settled to have temporal coincidence between probe and reference at the photodiode entrances.

The pump & probe technique requires the spatial and temporal characterization of both the pump and probe pulses at the focus of the microscope objective. While the spatial characterization has already been discussed in my previous thesis work [1], the temporal characterization will be developed in the following chapters.

[1] If the measurement is realized with a detuning of 1 kHz. Moreover to improve the ratio signal/noise the measurement must be integrated increasing the capturing time up to the order of minutes.

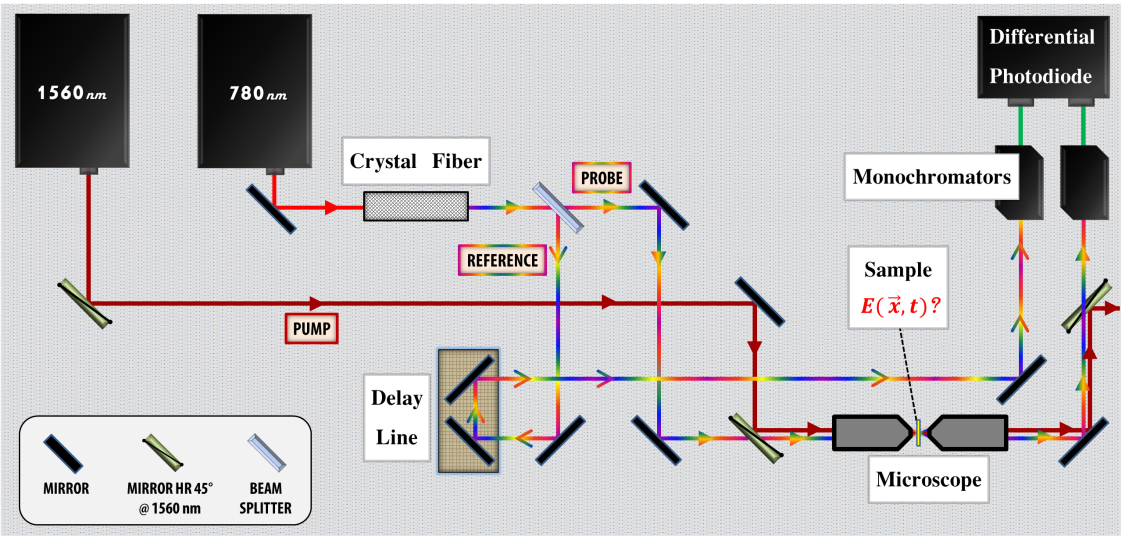

Figure 2.3: Reference experimental setup. This arrangements allows to follows the thermo-mechanical dynamics of a nanostructured sample exploiting the pump & probe technique with ASOPS and an appropriate tailored microscopy system. To makes the setup operative the complete characterization of the pump and probe pulses at the foci of the first microscope objective is required.

Chapter 3

Temporal characterization of an ultrashort laser pulse

In this Chapter we will explain what it is meant for a complete temporal characterization of a pulse and how this characterization can be achieved through the FROG technique. Here the FROG technique will be presented in two section: the first one will show the generic FROG experimental apparatus and the second one the working principle of the FROG phase-retrieval algorithm. Follow a section where will be discussed the main FROG geometries with the respective advantages and disadvantages.

3.1 Temporal characterization [13]

A pulse is completely characterized by its electric field in the temporal domain. The time dependent component of the pulse can be written as:

$$E(t) = \mathrm{Re}\left\{ \sqrt{I(t)}\, \exp(i\omega_0 t - i\varphi(t)) \right\}, \tag{3.1}$$

where $I(t)$, ω_0 and $\varphi(t)$ are the temporal intensity, the carrier frequency and the temporal phase of the pulse respectively. The instantaneous frequency of the pulse $\omega(t)$ is defined by

$$\omega(t) = \omega_0 - \frac{d\varphi}{dt}\,. \tag{3.2}$$

Therefore, a pulse with a constant temporal phase does not present phase variation in time. If the phase vary linearly in time, the frequency will be simply translated. Nevertheless, if the phase vary quadratically in time, the frequency will change linearly. In this case one can discern between "positively chirped" and "negatively chirped" pulses, where the frequency is increasing and decreasing respectively. When the phase distortion is simply quadratic, the chirp is said to be linear. Higherorder terms imply nonlinear chirp.

The pulse field can equally well be written in the frequency domain (neglecting the negative-frequency term)

$$\tilde{E}(\omega) = \sqrt{\tilde{I}(\omega - \omega_0)}\, \exp(i\tilde{\varphi}(\omega - \omega_0))\,, \tag{3.3}$$

where $\tilde{E}(\omega)$ is the Fourier transform of $E(t)$. $\tilde{I}(\omega - \omega_0)$ is the spectrum intensity and $\tilde{\varphi}(\omega - \omega_0)$ is the spectral phase. The spectral phase contains time versus frequency informations, and define the group delay versus frequency $\tilde{\tau}(\omega)$, which is given by

$$\tilde{t}(\omega) = \frac{d\tilde{\varphi}}{d\omega}\,. \tag{3.4}$$

As in the time domain, a constant spectral phase means no time variation with frequency. Linear variation of $\tilde{\varphi}(\omega - \omega_0)$ with frequency is simply a shift in time, that is, a delay. Quadratic variation of $\tilde{\varphi}(\omega - \omega_0)$ with frequency represent a linear ramp of group delay versus frequency, and corresponds to a pulse that is "linearly chirped". Also, as in the time domain, higher-order terms imply nonlinear chirp.

To characterized a pulse we desire to measure $E(t)$ (or $\tilde{E}(\omega)$) completely, that is, to measure both the intensity and phase, expressed in either domain. We must be able to do so even when the pulse has significant intensity structure and highly nonlinear chirp. In the frequency domain it is possible to measure the spectral intensity using a spectrometer, but not the spectral phase. In the time domain, it has not been possible to measure either intensity or phase because the femtosecond pulses are so much shorter than the temporal resolution of measurement devices. The main device available for time-domain characterization of an ultrashort pulse has been the autocorrelator, which, since no shorter event is available, uses the pulse to measure itself. Specifically, it involves splitting the pulse into two replicas, variably delaying one with respect to the other, and spatially overlapping the two pulses in some instantaneously responding nonlinear-optical medium, such as a second-harmonic-generation (SHG) crystal. A SHG crystal will produce a wave at twice the frequency of the input wave with an intensity that is proportional to the product of the intensities of the two input pulses. The second harmonic signal depends on the overlap in time between the two pulses and then it will be related to the input pulse length. Specifically, an autocorrelator yields

$$A(\tau) = \int_{-\infty}^{\infty} I(t)I(t-\tau)\, dt\,,$$

where τ is the relative delay between the pulses. Unfortunately, this measurement yields a "smeared out" version of $I(t)$, and it often hides structure. For example, a structure which contains several satellite pulses can be erroneously reconstructed as its envelope. Besides, in order to obtain information as the pulse length, a guess must be made as to the pulse shape, yielding a multiplicative factor that relates the autocorrelation full width at half-maximum to that of the pulse $I(t)$. Unfortunately, this factor varies significantly for different common pulse shapes. Moreover, even when the spectrum is also measured, there is not sufficient information to determine the pulse. Finally, in the

autocorrelation measurements can be present systematic error (misalignment effects can introduce distortions) and it is difficult to know when the measured autocorrelation is free of such effects. Despite these serious drawbacks, the autocorrelation and spectrum have remained the standard measures of ultrashort pulses until the beginning of the 90′, largely for lack of better methods.

Frequency-Resolved Optical Gating (FROG) is a technique introduced in the beginning of the 90′ with the purpose of measuring the intensity $I(t)$ and the phase $\varphi(t)$ of a single femtosecond pulse, i.e. its complex electric field $E(t)$. There are not required complicated apparatus: the FROG simply needs the spectral resolution of the signal from an autocorrelator. The system input must be a single ultrashort arbitrary optical pulse, whom we want to determine $E(t)$.
Throughout splitting of the pulse in two replicas, the use of an instantaneous responding non-linear optical medium and a spectrometer is generated the FROG trace $I(\omega, \tau)$, that express the intensity versus the frequency and the delay between the replicas. With the FROG trace, one can lay out a phase retrieval problem $\varphi(t)$ that can be solved by means of an iterative algorithm based on the Fourier transform. The algorithm uses the FROG trace as data input, while as constraint must be indicated the shape of the signal field $E_{sig}(t, \tau)$ produced in the non-linear interaction, which depends on the working geometry chosen.

FROG overcomes the typical limitations of the standard techniques. It can determining the intensity and phase evolution of an ultrashort arbitrary pulse from a single pulse or a pulse train. The experimental apparatus is simple and it can be assembled in a single day once that all the components are available. As most ultrafast laboratories already possess an autocorrelator and spectrometer for pulse measurement, complete pulse measurement using FROG requires no new apparatus. Since FROG works in phase-matching mode, it does not need any critical alignment. FROG has been tested in the ultraviolet, visible and infrared for pulses from 20 kW to 1 GW (from 2 nJ to 100 μJ for a pulse of 100 fs). It has been demonstrated with single and multiple pulse configuration and it has been proved on various pulse shapes (like pulses with a linear chirp or a cubic distortion in the phase).

FROG can be contextualized in two parts: the first one is the experimental apparatus where two replicas of the pulse to measure are overlapped in a non-linear optical mean, which yields a signal that, resolved in frequency and in the delay time between the replicas, generates the FROG trace; the second one is a phase retrieval algorithm, that extracts the intensity and phase evolution from the experimental FROG trace.

3.2 Experimental apparatus [14] [15]

A possible working system is schematically reported in Figure (3.1). The general experimental system requires an incoming ultrashort optical pulse, which is characterized by the complex electric field $E_i(t)$ that we want measure. Through a beam-splitter two replicas of the input pulse are generated. By the use of a delay line, it is possible to produce a temporal delay τ between the two replica pulses: the probe pulse will be

characterized by an electric field $E(t)$, while the gate pulse will present a retarded field $E(t-\tau)$. With a lens system the two replica pulses are focused into a non-linear optical mean, whom effects must be instantaneous. The output of the optical mean is a signal pulse, whom electric field $E_{sig}(t,\tau)$ depends on the dominant non-linear effect. Under the hypotheses of instantaneous response of the optical mean (neglecting the effects of the temporal dispersion), plane waves (neglecting the effects of the group velocity mismatch between the two replica pulses) and perfect phase-matching (neglecting the effects of a finite coherence length between the two replica waves), the signal pulse field $E_{sig}(t,\tau)$ has the generic form

$$E_{sig}(t,\tau) \sim E(t)\, g(t-\tau)\,, \tag{3.5}$$

where $g(t-\tau)$ is the gate function and it is defined by the non-linear effect. Here, the proportionality constants are not reported in the formulas because they will be experimentally determined. What we are interested in is the shape of the signal versus time. Working with some object lens the signal is focused into the spectrometer fissure. Finally, operating with a CCD camera, it is possible to reconstruct the experimental trace, known as the FROG trace, that consists in a measure of the spectral intensity in function of the delay

$$I_{FROG}(\omega,\tau) \sim |E_{sig}(\omega,\tau)|^2 \sim \left| \int_{-\infty}^{+\infty} E_s(t,\tau)\, e^{-i\omega t}\, dt \right|^2 \tag{3.6}$$

which, according to Eq. 3.5, has the shape

$$I_{FROG}(\omega,\tau) \sim \left| \int_{-\infty}^{+\infty} E(t)\, g(t-\tau)\, e^{-i\omega t}\, dt \right|^2 . \tag{3.7}$$

Experimentally, the FROG trace collected by the CCD camera consists in a squared matrix $N{\times}N$. The non-linear mechanism needed to generate the FROG trace depends on the chosen geometry. The main request is that the effect must be instantaneous. In the case of a geometry like the one in Figure (3.1), where it has been used a second-harmonic crystal, the dominant effect is the second-harmonic generation (SHG). In this case one refers to the system as SHG FROG, and the gate function becomes $g(t-\tau) = E(t-\tau)$. Following Eq. (3.5), the signal pulse field can be written as

$$E_{sig}^{SHG}(t,\tau) \sim E(t)\, E(t-\tau)\,. \tag{3.8}$$

It present a carrier frequency that will be doubled in respect to the probe pulse.

The FROG trace requires time and frequency resolution simultaneously, and it contains sufficient informations to the complete determination of the field $E(t)$. Mathematically, the FROG trace of Eq. (3.7) is the spectrogram of $E(t)$, therefore it is an expression of the spectral components of $E(t)$ filtered through the gate function $g(t-\tau)$ varying the delay τ. The knowledge of the spectrogram of $E(t)$ is essentially sufficient to

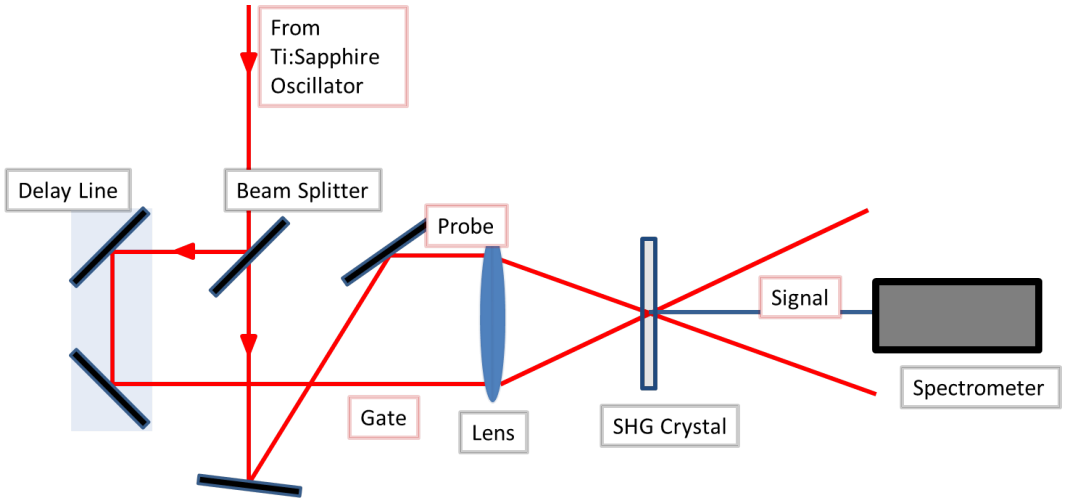

Figure 3.1: SHG FROG. In this geometry: a pulsed laser beam is duplicated through a beam-splitter; the pulsed beam that continue below is called probe; the pulsed beam that go inside the delay line is called gate; the two pulses are focused in a second-harmonic crystal, so that both their foci are spatially overlapped inside the mean; the spectrometer measure the intensity in function of the frequency; varying the delay of the gate field one measure the intensity in function of the delay.

completely define $E(t)$ (unless an arbitrary phase factor, which is not relevant in optical problems).

The use of the gate pulse itself to generate the gate function of the spectrogram is necessary to have a sufficient temporal resolution. Anyway, the problem becomes more complicate somewhat. Spectrogram inversion algorithms require knowledge of the gate function and hence cannot be used. The problem must then be recast into another form. The solution is to rewrite the expression of Eq. (3.7) as the "two-dimensional phase-retrieval problem."

Now, consider $E_{sig}(t,\tau)$ of the Eq. (3.5) to be the Fourier transform with respect to t of a new quantity that we will call $E_{sig}(t,\Omega)$. It is important to note that, once found, $E_{sig}(t,\Omega)$ easily yields the pulse field, $E(t)$. Specifically, $E(t) = E_{sig}(t,\Omega = 0)$ (a complex multiplicative constant remains unknown, but is of little interest). Thus, to measure $E(t)$, it is sufficient to find $E_{sig}(t,\Omega)$.

According with l'Eq. (3.7), we can rewrite the expression for the FROG trace in terms of $E_{sig}(t,\Omega)$

$$I_{FROG}(\omega,\tau) \sim \left| \int_{-\infty}^{+\infty} E_{sig}(t,\Omega)\, e^{-i\omega t - i\Omega\tau}\, dt\, d\Omega \right|^2 . \tag{3.9}$$

Here, we see that the measured quantity, $I_{FROG}(\omega,\tau))$, is the squared magnitude of the 2D Fourier transform of $E_{sig}(t,\Omega)$. The spectrogram measurement thus yields the magnitude, but not the phase, of $E_{sig}(t,\Omega)$, the two-dimensional Fourier transform of

the desired quantity $E(t)$. The problem is then to find the phase of the Fourier transform of $E_{sig}(t, \Omega)$. This is the 2D phase-retrieval problem.

The problem can be solved in case certain additional information regarding $E_{sig}(t, \Omega)$ is available (such as a finite support, outside whom the function is zero for every t and Ω). (Note how this is not possible in the 1D problem, where it is impossible to find a function of one variable whom Fourier transform magnitude known, despite additional information, such as finite support. Indeed, in the 1D case, infinitely many additional solutions exist). In the ultrashort pulses measurements, the required additional information consists in the knowledge of the mathematical shape of $E_{sig}(t, \Omega)$, rather then in the finite support. For example, in SHG FROG, we know that $E_{sig}(t, \tau) \sim E(t)\, E(t - \tau)$. This additional information turns out to be sufficient, and thus, the problem is formally solved. It is possible to develop a phase-retrieval algorithm to pick out the solution $E(t)$. The constraint regarding the mathematical shape of the signal field $E_{sig}(t, \tau)$ is strong enough to assist the convergence.

3.3 FROG phase-retrieval algorithm [14] [15] [13]

To retrieve the pulse electric field $E(t)$ from the FROG trace associated it is necessary the introduction of an iterative algorithm based on the Fourier transform. To be thorough, must be pointed out that the algorithm works, but it has not been formally demonstrated yet. The algorithm is needed to treat the phase-retrieval problem. In the generic phase-retrieval problem one desires to reconstruct an image starting from two informations:

1. the Fourier transform magnitude of the image,
2. a constraint on the image domain.

In the specific case:

1. the image $E_{sig}(\omega, \tau)$ is modified in such a way to have the same intensity of the experimental data $I_{FROG}(\omega, \tau)$:
$$I_{FROG}(\omega, \tau) = |E_{sig}(\omega, \tau)|^2 = \left| \int E_{sig}(t, \tau) e^{i\omega t}\, dt \right|^2 , \tag{3.10}$$
2. the shape of the signal field $E_{sig}(t, \tau)$ is defined on the knowledge of the non-linear process that yields to it:
$$E_{sig}(\omega, \tau) = E(t)\, g(t - \tau) . \tag{3.11}$$

The beginning cycle of the algorithm will be described with reference to the diagram of Figure (3.2).

- The process start with the choice of an initial guess for the pulse complex electric field $E(t)$ (typically, it is used a slowly variable intensity shape, as a Gaussian distribution, and a phase Random distribution). The introduction of a particular initial guess to make the algorithm begin to run, does not impose any constriction

on the nature of the pulse field we want to obtain; indeed, the algorithm result is independent on the particular initial guess; it will change only the cycle numbers required to converge to the result. Numerically, $E(t)$ is stored as a vector of N elements. It is important to check that the field has a negligible intensity outside the domain defined by the vector.

- The initial guess $E(t)$ is exploited to generate the signal field $E_{sig}(t,\tau)$, which will be dependent on the dominant non-linear process (point 2 above).
- Operating the Fourier transform (FT) on the signal field, one get $E_{sig}(\omega,\tau)$.
- The magnitude of this results is replaced by the one associated to the FROG trace $I_{FROG}(\omega,\tau)$ (point 1 above)

$$E_{sig}(\omega,\tau) \quad \longrightarrow \quad E'_{sig}(\omega,\tau) = \frac{E_{sig}(\omega,\tau)}{|E_{sig}(\omega,\tau)|}\sqrt{I_{FROG}(\omega,\tau)}\,.$$

  This substitution change the amplitude, but not the phase which is kept fixed. Typically, one works with a FROG trace $I_{FROG}(\omega,\tau)$ with dimensions $N\times N$. It is important to check that the FROG trace has a negligible intensity outside the domain defined by the matrix.
- Operating the reverse Fourier transform (IFT) on $E'_{sig}(\omega,\tau)$, one get $E'_{sig}(t,\tau)$.
- To close the cycle, one generate a new version of the pulse complex field $E'(t)$, integrating the new signal field $E'_{sig}(t,\tau)$ over the delay τ

$$\int_{-\infty}^{+\infty} E'_{sig}(t,\tau)\,d\tau = E'(t)\int_{-\infty}^{+\infty} g'(t-\tau)\,d\tau = E'(t)\;G\,,$$

  where G is a real constant.
- N.B. These last two points should be inverted to increase the algorithm speed. Indeed, integrating before and applying the IFT after, one gets the same result $E'(t)$. Yet, in this way, the number of IFT is reduced from N to 1.
- The second cycle begins taking $E'(t)$ as the initial guess.
- In every cycle, the pulse electric field get closer and closer to the true value.
- The k-th cycle will start with the initial guess $E^{(k-1)}(t)$. When $E^{(k-1)}(t) = E^{(k-2)}(t)$ the process will stop: there is convergence to the vector $E^{(k-1)}(t)$.

In theoretical simulations, where the pulse field $E(t)$ is known, we define the error of the field E

$$\mathcal{E}_E^{(k)} = \sqrt{\frac{1}{N}\sum_{i=1}^{N}\left|E^{(k)}(t_i) - E(t_i)\right|^2}\,, \tag{3.12}$$

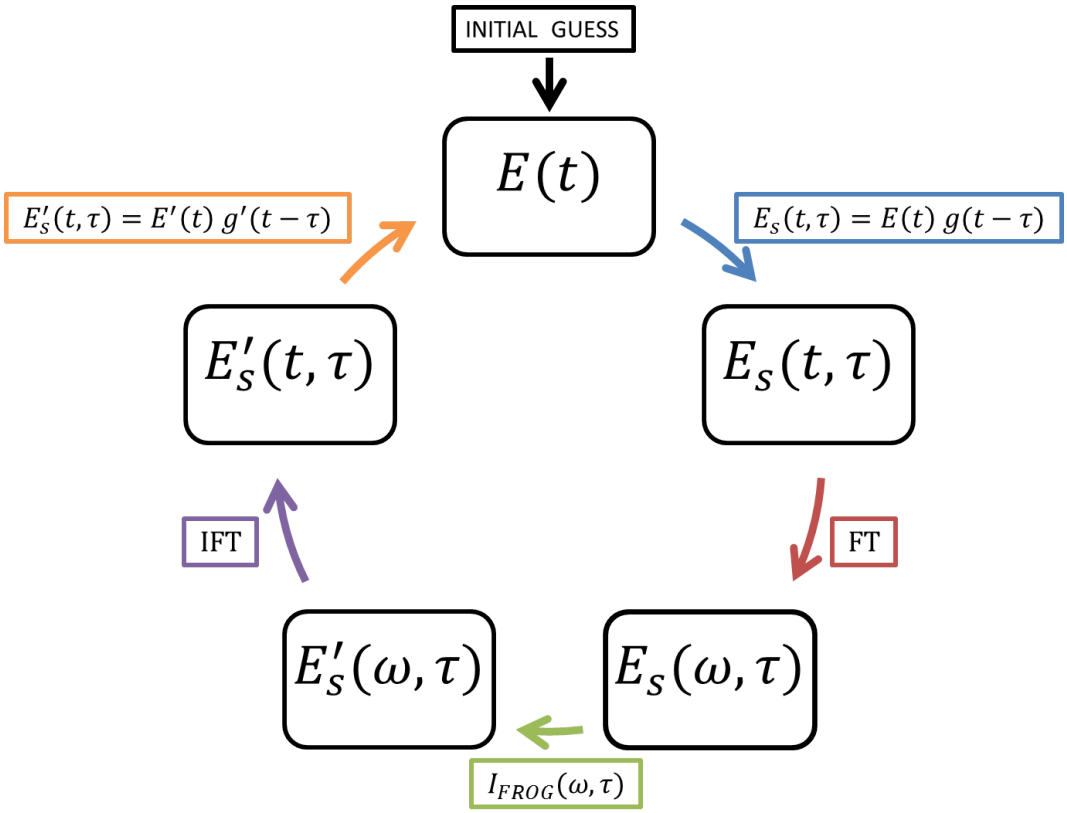

Figure 3.2: Diagram about the first algorithm cycle. The cycle begins with an initial guess for $E(t)$; exploiting the knowledge of the non-linear effect one gets the signal shape $E_{sig}(t,\tau)$; operating the Fourier transform one passes in the frequency domain $E_{sig}(\omega,\tau)$; applying the FROG experimental data one redefines the amplitude (the phase is kept) $E'_{sig}(\omega,\tau)$; Realizing the reverse Fourier transform one goes back to the time domain $E'_{sig}(t,\tau)$; integrating over all the delays one gets a new guess for $E(t)$, which it will be used in the following cycle.

where $E^{(k)}(t_i)$ is the i-th component of the field vector gotten at the end of the k-th cycle, while $E(t_i)$ is the i-th component of the field vector. To keep into account the trivial ambiguities (arbitrary constant phase) it is necessary to translate $E^{(k)}(t_i)$ and $E(t_i)$ so that in both of them the maximum is placed at the half of the vector t ($i = \frac{N}{2} + \frac{1}{2}$ in case N is odd). Normalizing both $E^{(k)}(t_i)$ and $E(t_i)$ so that their absolute maximum is unitary, $\mathcal{E}_E^{(k)}$ become the percentage error of E.

In experimental situations, where the pulse field $E(t)$ is unknown, we define the error of the field E

$$\mathcal{E}_{FROG}^{(k)} = \sqrt{\frac{1}{N^2}\sum_{i=1}^{N}\sum_{j=1}^{N}\left[I_{FROG}^{(k)}(\omega_i,\tau_j) - I_{FROG}(\omega_i,\tau_j)\right]^2}, \tag{3.13}$$

where $I^{(k)}_{FROG}(\omega_i, \tau_j)$ is the FROG trace yields in the end of the k-th iteration, while $I_{FROG}(\omega_i, \tau_j)$ is the FROG trace. Normalizing these two quantities, so that they have unitary absolute maximum, $\mathcal{E}^{(k)}_{FROG}$ becomes the percentage error of I_{FROG}. The Eq. (3.13) gives a mean to state how the k-th guess $E^{(k)}(t)$ is near to the field that has generated the FROG trace $I_{FROG}(\omega, \tau)$. The formula is based on the correspondence 1 to 1 that exists between fields and FROG traces.

The algorithmic method described above is called generalized projections, and it is frequently used in phase-retrieval problems unrelated to FROG. The essence of the generalized projections technique is graphically displayed in Figure (3.3). Consider Figure (3.3) as a Venn diagram in which the entire figure represents the set of all complex functions of two variables, i.e., potential signal fields, $E_{sig}(t, \tau)$. The signal fields satisfying the data constraint, Eq. (3.10), are indicated by the lower elliptical region, while those satisfying the mathematical-form constraint, Eq. (3.11), are indicated by the upper elliptical region. The signal pulse field satisfying both constraints, the intersection of the two elliptical regions, is the solution. And it uniquely yields the pulse field, $E(t)$.

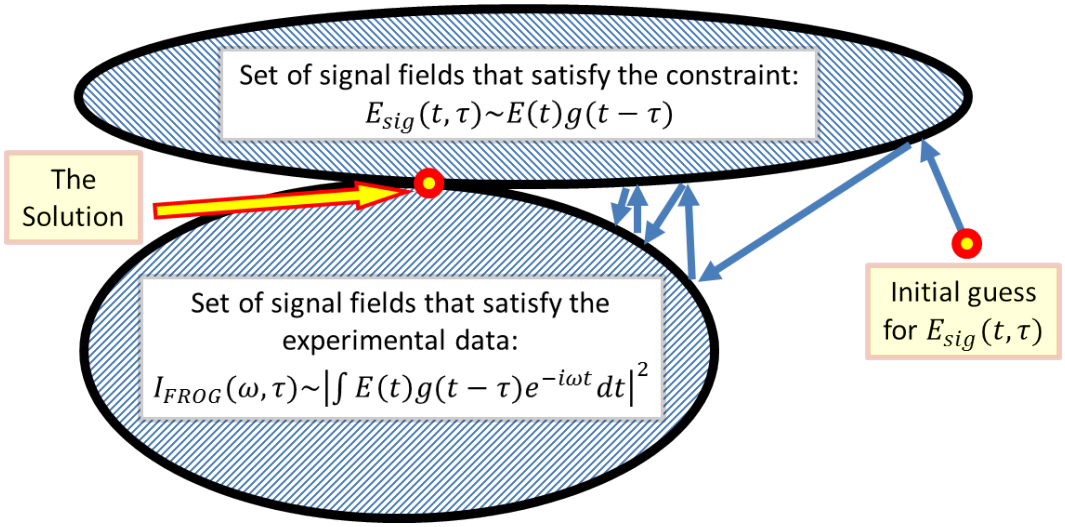

Figure 3.3: Geometrical interpretation of the generalized-projections iterative algorithm, showing that convergence to the correct result is guaranteed when the constraint sets are convex. Convergence remains highly likely even when the sets are not convex, as is the case in FROG.

The solution is found by making "projections", which have simple geometrical analogs. We begin with an initial guess at an arbitrary point in signal-field space. We then make a projection onto one of the constraint sets, which consists of moving to the closest point in that set to the initial guess. Call this point the first iteration. From this point, we then project onto the other set, moving to the closest point in that set to the first iteration. This process is continued until the solution is reached. When the two constraint sets are convex (all line segments connecting two points in each constraint set lie entirely within the set), then convergence is guaranteed.

Unfortunately, the constraint sets in FROG are not convex. When a set is not convex, the projection is not necessarily unique, and a "generalized projection" must be defined. The technique is then called generalized projections, and convergence cannot be guaranteed. On the other hand, the error of between the FROG trace the current signal field and the measured FROG trace, Eq. (3.13), can be shown to continually decrease with iteration number, and, although it is conceivable that the algorithm may stagnate at a constant value, this approach is quite robust in FROG problems. And, when combined with other algorithmic methods, it is extremely robust.

3.4 FROG geometries [13] [16] [17]

In this section, we describe and compare several FROG beam geometries and their traces, so that the choice of which geometry to use may be more easily made. There are different version of FROG, which rely on different non-linear gating mechanism, generating different kinds of FROG traces (thus requiring different phase retrieval algorithms), and have different strengths and weaknesses. The better FROG geometry that is required in the measurement depends mainly on the pulse characteristics (like power, carrier frequency, temporal and spectral width).

3.4.1 PG FROG

Polarization-gate FROG (PG FROG) is the conceptually simplest FROG variant and uses the configuration shown in Fig. (3.4). In this geometry, the pulse is split into two, with one pulse (the probe) sent through crossed polarizers and the other (the gate) through a half-wave plate in order to achieve a $\pm 45^\circ$ linear polarization with respect to that of the probe pulse. The two pulses are then spatially overlapped in a medium with a very fast third-order susceptibility (e.g. fused silica). In the medium, the gate pulse induces a birefringence through the electronic Kerr effect, a third-order optical non-linearity, also known as the non-linear refractive index. As a result, the medium acts as a wave plate while the gate pulse is present, rotating the probe pulse's polarization slightly, which allows some light to be transmitted throughout the second polarizer. Because birefringence occurs only when the gate pulse is present, this geometry yields an autocorrelation measurement of the pulse if one simply measures the intensity of the light transmitted throughout the second polarizer versus the relative delay between the two pulses. And by spectrally resolving the light transmitted versus delay, a PG FROG trace is measured.

The PG FROG trace is given by

$$I_{FROG}^{PG}(\omega,\tau) \sim \left| \int_{-\infty}^{+\infty} E(t)\ |E(t-\tau)|^2\ e^{-i\omega t}\, dt \right|^2 . \tag{3.14}$$

Note that the gate function in PG FROG is $|E(t-\tau)|^2$, which is a real quantity and so adds no phase information to the gated slice of $E(t)$ whose spectrum is measured.

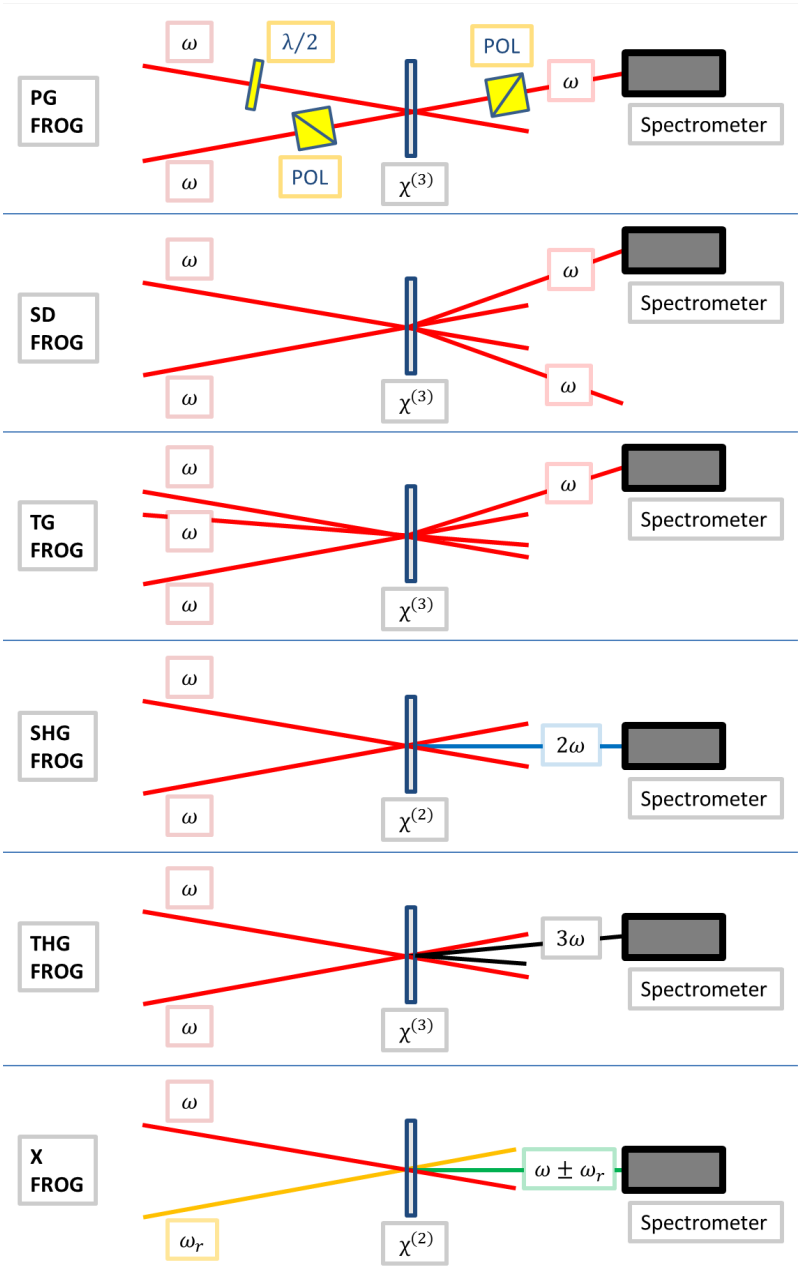

Figure 3.4: Schematics of six different beam geometries for performing FROG measurements of ultrashort laser pulses: polarization gate (PG), self-diffraction (SD), transient grating (TG), second-harmonic generation (SHG), third-harmonic generation (THG), and cross-correlation (X) FROG. On the left are indicated the input pulses; on the right is indicated the signal pulse directed towards the spectrometer; the non-linearity of the non-linear medium is shown; POL=polarizer; $\lambda/2$=half-wave plate. Not shown are delay lines and various lenses. The frequencies shown ($\omega, \omega_r, 2\omega, 3\omega$) are the carrier frequencies of the pulses involved and indicate whether the signal pulse has the same carrier frequency as the input pulse or is shifted, as in SHG, THG and XFROG.

As a result, PG FROG traces are quite intuitive, accurately reflecting the instantaneous pulse frequency of Eq. (3.2) versus time.

Overall:

- Advantages of PG FROG are the generation of a fairly intuitive FROG traces, easy alignment due to an automatically phase-matched non-linear process and, most importantly, the absence of ambiguities in the retrieval which leads to a complete unambiguous pulse characterization.
- Disadvantages of PG FROG are that it requires high-quality polarizers (an extinction coefficient of better than 10^{-5} is recommended), which can be expensive. In addition, high-quality polarizers tend to be fairly thick, so pulses can change due to material dispersion while propagating through them. A further disadvantage of the requirement of high-quality polarizers is that they are unavailable in spectral regions such as the deep UV ($\lesssim$190 nm). They also limit sensitivity because there is always some leakage. However, these disadvantages are not severe, especially for amplified ultrashort pulses in the visible and the near-IR.
- Useful for measuring long pulses (specially in the single-shot geometry, where the automatic phase-matching of the process allows for large crossing angles and hence large delay ranges).

3.4.2 SD FROG

Self-diffraction FROG (SD FROG) is another beam geometry that uses the electronic Kerr effect as the non-linear optical process for making optical gating in FROG measurements, and uses the configuration shown in Fig. (3.4). SD FROG also involves crossing two beams in a third-order nonlinear medium, but in SD FROG, the beams can have the same polarizations. The beams generate a sinusoidal intensity pattern and hence induce a material grating, which diffracts each beam into the directions shown in Fig. (3.4). Spectrally resolving one of these beams as a function of delay yields an SD FROG trace.

The expression for the SD FROG trace is

$$I_{FROG}^{SD}(\omega,\tau) \sim \left| \int_{-\infty}^{+\infty} E^2(t)\, E^*(t-\tau)\, e^{-i\omega t}\, dt \right|^2 . \tag{3.15}$$

SD FROG traces differ slightly from PG FROG traces. For a linearly chirped pulse, the slope of the SD FROG trace is twice that of the PG FROG trace. As a result, SD FROG is more sensitive to this and other even-order temporal-phase distortions. It is, however, less sensitive to odd-order temporal-phase distortions. SD FROG also uniquely determines the pulse intensity and phase.

A strength of SD FROG over PG FROG is that it does not require polarizers, so it can be used for deep UV pulses or pulses that are extremely short. On the other hand, SD is not a phase-matched process. As a result, the nonlinear medium must be kept thin ($\lesssim 200\,\mu$m) and the angle between the beams small ($\lesssim 2^\circ$) in order to minimize the phase-mismatch. In addition, the phase-mismatch is wavelength dependent. Consequently,

if the pulse bandwidth is large, the SD process can introduce wavelength-dependent inefficiencies into the trace, resulting in distortions. These pitfalls are easily avoided for ≥ 100 fs pulses.

Summarizing:

- Advantages of SD FROG are the generation of a fairly intuitive FROG traces and the absence of cross polarizers (can be used in the deep UV).
- Disadvantages of SD FROG are tied to the non-phase-matched mode of the process, e.g. are required relatively long pulse's temporal lengths, high pulse intensities, thin mediums, small angles between the beams.
- Useful for measuring UV and extremely short pulses (as it involves minimal propagation through optical components).

3.4.3 TG FROG

Transient-grating FROG (TG FROG) is a geometry that is both phase matched and free of polarizers, and uses the configuration shown in Fig. (3.4). TG FROG is a three-beam geometry, requiring that the input pulse be split into three pulses. Two of the pulses are overlapped in time and space at the optical-Kerr medium, producing a refractive-index grating, just as in SD FROG. In TG, however, the third pulse is variably delayed and overlapped in the medium and is diffracted by the induced grating to produce the signal pulse. The four beam angles (three input and one output) in TG geometries usually take the form of what is known as the "BOXCARS" arrangement, in which all input pulses and the signal pulse are nearly collinear, but appear as spots in the corners of a rectangle on a card placed in the beams. All four beams should be nearly co-propagating in order to avoid temporal smearing effects due to large beam angles.

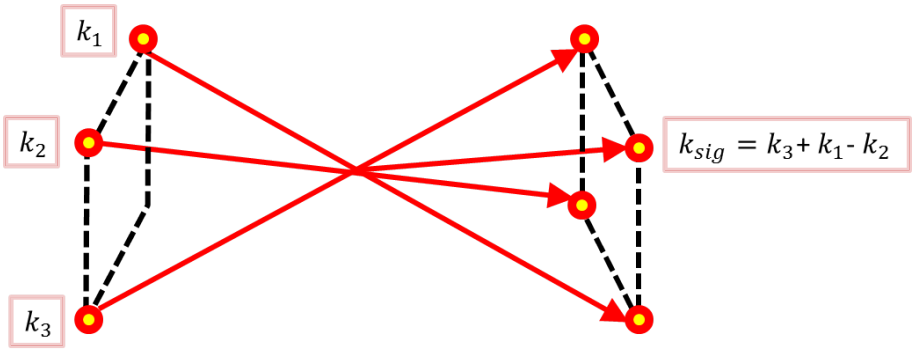

Figure 3.5: The input pulses are numbered 1, 2, and 3, and "sig" indicates the signal pulse. In a "BOXCARS" beam geometry each pulse propagates at the corner of a rectangle. All pulses should propagate in nearly the same direction to avoid temporal smearing. Two pulses should be coincident in time, while the other has variable delay.

The TG FROG trace is mathematically equivalent to PG FROG or SD FROG, depending on which pulse is variably delayed. For example, if pulse number two on Fig.

(3.4) is variably delayed, the TG FROG trace is given by

$$I_{FROG}^{TG_2}(\omega,\tau) \sim \left| \int_{-\infty}^{+\infty} E_1(t)\, E_2^*(t-\tau)\, E_3(t)\, e^{-i\omega t}\, dt \right|^2 ,$$

but since we are in the degenerate case, this becomes

$$I_{FROG}^{TG_2}(\omega,\tau) \sim \left| \int_{-\infty}^{+\infty} E^2(t)\, E^*(t-\tau)\, e^{-i\omega t}\, dt \right|^2 \tag{3.16}$$

which is just the expression for the SD FROG trace. On the other hand, if the variably delayed pulse is number one or three, the TG FROG trace is equivalent to the PG one

$$I_{FROG}^{TG_1}(\omega,\tau) \sim \left| \int_{-\infty}^{+\infty} E(t)\, |E(t-\tau)|^2\, e^{-i\omega t}\, dt \right|^2 . \tag{3.17}$$

TG FROG has several advantages over its two-beam cousins. Unlike PG FROG, it avoids polarizers, so it does not distort extremely short pulses, and hence can be used in the deep UV. It can use all parallel polarizations, which yields greater signal strength because the $\chi^{(3)}_{1111}$ element of the susceptibility tensor is a factor of three larger than the off-diagonal elements used in PG FROG. This fact, coupled with the lack of polarizer-leakage background, makes TG FROG significantly more sensitive than PG FROG. Unlike SD FROG, TG FROG is phase-matched, so long interaction lengths in the non-linear medium may be used, enhancing signal strength due to the length-squared dependence of the signal intensity. In addition, larger beam angles may be used than in SD FROG, reducing any scattered-light background. As a result, TG FROG is also significantly more sensitive than SD FROG. At the same time, TG FROG retains the intuitive traces and ambiguity-free operation common to these two-beam FROG methods.

The only weakness of TG FROG is the need for three beams and to maintain good temporal overlap of the two constant-delay beams. Anyway, these requirements are not particularly inconvenient, and the advantages of this geometry far outweigh the disadvantages.

Summarizing:

- Advantages of TG FROG are the generation of a fairly intuitive FROG traces, the absence of cross polarizers (can be used in the deep UV and in background-free measures), the phase-matched mode of the process (possibility of working with shorter pulses, lower pulse intensities, longer mediums, bigger angles between the beams).
- Disadvantage of TG FROG is the requirement of three beams.
- Useful for measuring extremely short pulses (~ 20 fs) of a few tens of nJ or more (thanks to the absence of polarizers and to the large phase-matched bandwidth).

3.4.4 SHG FROG

Second-harmonic-generation FROG (SHG FROG) is the most popular FROG variant and it uses the scheme shown in (3.4).

SHG FROG is a two beam geometry that, exploiting the second-harmonic generation process, yields a SHG trace

$$I_{FROG}^{SHG}(\omega,\tau) \sim \left| \int_{-\infty}^{+\infty} E(t)\, E(t-\tau)\, e^{-i\omega t}\, dt \right|^2 , \tag{3.18}$$

as mentioned in Sec. 3.2.

Fig. (3.1) shows a typical SHG FROG apparatus, consisting of a beam splitter, a delay line on translation stages to give variable delays, a 10- to 50-cm-focal-length lens to focus the pulses into the SHG crystal (usually KDP or BBO), and a spectrometer. The crystal thickness for measuring 100 fs, 800 nm pulses should be no more than $\sim$300 mm for KDP and $\sim$100 mm for BBO.

The main advantage of SHG FROG is sensitivity: it involves only a second-order nonlinearity, while the previously mentioned FROG variations use third-order optical nonlinearities, which are much weaker. As a result, for a given amount of input pulse energy, SHG FROG will yield more signal pulse energy. SHG FROG is commonly used to measure unamplified pulses directly from a Ti:Sapphire oscillator, and it can measure pulses as weak as about 1 pJ; it is only slightly less sensitive than an autocorrelator.

The main disadvantages of SHG FROG are that, unlike the previously mentioned third-order versions of FROG, it has an unintuitive trace that is symmetrical with respect to delay, and, as a result, it has an ambiguity in the direction of time. The pulse field, $E(t)$, and its time-reversed replica, $E(-t)$, both yield the same SHG FROG trace. Thus, when an SHG FROG trace is measured and the phase-retrieval algorithm run on it, it is possible that the actual pulse is the time-reversed version of the retrieved pulse. This ambiguity can easily be removed in one of several ways. One is to make a second SHG FROG measurement of the pulse after distorting it in some known manner. The most common method is to place a piece of glass in the beam (before the beam splitter), introducing some positive dispersion and hence chirp into the pulse. Only one of the two possible pulses is consistent with both measurements. Another is to know in advance something about the pulse, such as that it is positively chirped. Finally, placing a thin piece of glass in the pulse before the beam splitter so that surface reflections introduce a small trailing satellite pulse also removes the ambiguity. This method has the advantage of requiring only one SHG FROG trace measurement to determine the pulse (the time-reversed pulse in this case has a leading satellite pulse). Beyond the time direction ambiguity, there is another class of ambiguities in SHG FROG. These ambiguities rarely appear in practical measurements but are worth mentioning. If the pulse consists of two (or more) well separated pulses, then the relative phase of the pulses has an ambiguity. Specifically, the relative phases, φ and $\varphi+\pi$, yield the same SHG FROG trace and hence cannot be distinguished.

The most important experimental consideration in SHG FROG is that the SHG crystal have sufficient bandwidth (i.e., be thin enough, since the bandwidth is inversely

proportional to the crystal thickness) to frequency double the entire bandwidth of the pulse to be measured. If the crystal is too thick, then the SHG FROG trace will be too narrow along the spectral axis, leading to non-convergence of the algorithm. Because the signal is generated at a frequency different than that of the input light, scattering is not a problem. However, one is limited in the maximum length of the crystal that one can use because of group-velocity mismatch.

Summarizing:

- Advantages of SHG FROG are the use of a $\chi^{(2)}$ non-linear crystal (much higher sensitivity than $\chi^{(3)}$ FROG versions), the absence of cross polarizers, the phase-matched mode of the process, the absence of scattering (since the signal frequency is different from the input frequencies).
- Disadvantages of the SHG FROG are the generation of unintuitive FROG traces and the ambiguity concerning the direction of time (which can be removed e.g. performing an additional measurement with some glass piece in the beam path), the limitation of the wavelength range, the limitation of the maximum length of the crystal (because of group-velocity mismatch).
- Useful for measuring unamplified low-energy pulses ($\lesssim 10\,\mathrm{nJ}$ for a $100\,\mathrm{fs}$ pulse) with wavelength range limited ($\gtrsim 380\,\mathrm{nm}$).

3.4.5 THG FROG

Third-harmonic-generation FROG (THG FROG) uses third-harmonic generation as the non-linear optical process in a FROG apparatus and Fig. (3.4) shows the arrangement required.

The expression for the THG FROG trace can be

$$I_{FROG}^{THG}(\omega,\tau) \sim \left| \int_{-\infty}^{+\infty} E^2(t)\, E(t-\tau)\, e^{-i\omega t}\, dt \right|^2 , \tag{3.19}$$

or

$$I_{FROG}^{THG}(\omega,\tau) \sim \left| \int_{-\infty}^{+\infty} E(t)\, E^2(t-\tau)\, e^{-i\omega t}\, dt \right|^2 ,$$

depending on the choice of the signal beam (between the two) that is spectrally resolved in the THG FROG measurements. Practically this choice is irrelevant.

The main advantage of THG FROG is that, like the other third-order FROG methods, it removes the direction-of-time ambiguity that occurs in SHG FROG. In addition, using surface-third-harmonic generation FROG (STHG FROG), the non-linear effect is sufficiently strong allowing to measure unamplified pulses from a Ti:Sapphire oscillator. Indeed, the only third-order FROG method to achieve this measurement has been STHG FROG.

In terms of its performance, THG FROG is intermediate between SHG FROG and the other third-order FROG methods. It is less sensitive than SHG FROG, but more sensitive than PG and SD FROG. Its traces are unintuitive, similar to SHG FROG traces, but they have a slight asymmetry that distinguishes them from SHG FROG traces and

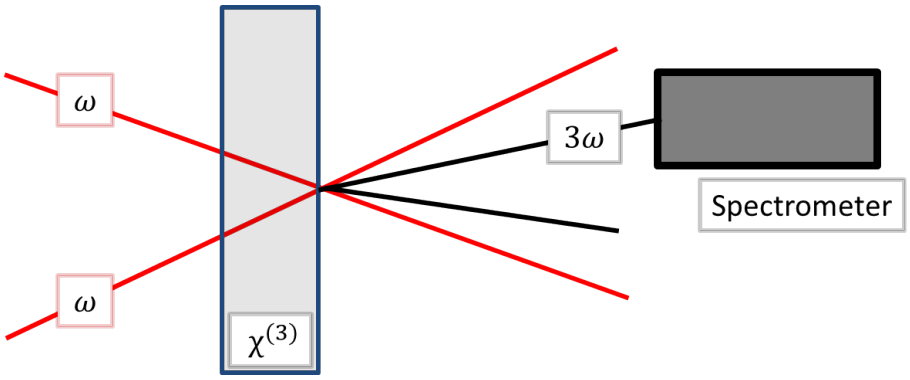

Figure 3.6: In the experimental apparatus for STHG FROG the two pulses overlap spatially at the exit face of the medium.

removes the direction-of-time ambiguity. On the other hand, THG FROG traces are not as intuitive as the other third-order FROG traces. And while THG FROG lacks the direction-of-time ambiguity of SHG FROG, it does have relative-phase ambiguities with well-separated multiple pulses, as is the case for SHG FROG. Thus, THG FROG and its special case, STHG FROG, represent a compromise between other FROG variations and hence may best be used only in special cases, such as for the measurement of an unamplified oscillator pulse train when only one trace can be made, and direction-of-time ambiguity is unacceptable.

However, there is a unique advantage to STHG FROG: the THG interaction is a surface effect, so the phase-matching bandwidth is extremely large. As a result, STHG FROG may be ideal for extremely short laser pulses, which require such a thin SHG crystal that SHG FROG measurements are difficult. For example, 10 fs pulses at 800 nm require a KDP crystal with a thickness of about 30 mm or less, which can be difficult to obtain. Thinner crystals represent even greater challenges. Consequently, Ti:Sapphire pulses $\sim$5 fs in duration may best be measured with STHG FROG.

Summarizing:

- Advantages of THG FROG are the absence of cross polarizers, the sensibility (higher than any other $\chi^{(3)}$ process), the large phase-matching bandwidth (in STHG), the absence of scattering (since the signal frequency is different from the input frequencies).

- Disadvantages of the THG FROG is the generation of unintuitive FROG traces, the limitation of the wavelength range, the limitation of the maximum length of the crystal (because of group-velocity mismatch).

- Useful for measuring unamplified extremely short pulses ($\sim$5 fs) at 800 nm (thanks to the absence of polarizers and to the extremely large phase-matched bandwidth), with wavelength range limited ($\gtrsim$570 nm).

3.4.6 XFROG

The well-characterized reference pulse can also be exploited through the cross-correlation FROG (XFROG). In XFROG, rather than create two replicas of the unknown pulse, we take the unknown pulse and the reference pulse, and cross them in the nonlinear optical medium. The produced trace will then be a true spectrogram. Only minor modifications to the FROG algorithm are required to retrieve the pulse intensity and phase from the XFROG trace, while retaining all the nice features of FROG.

Cross-correlation FROG (XFROG), rather than create two replicas of the unknown pulse, uses a known reference pulse which does not need to be spectrally overlapping with the pulse under investigation. The relative configuration is shown in (3.4). In brief, XFROG takes the unknown pulse and the reference pulse, and crosses them in the nonlinear optical medium. The produced trace will then be a true spectrogram. Only minor modifications to the FROG algorithm are required to retrieve the pulse intensity and phase from the XFROG trace, while retaining all the nice features of FROG.

Depending on the relative frequencies of the pulses, sum frequency generation (SFG), difference frequency generation (DFG), or a host of third-order processes can be used to create the cross-correlation signal. The electric field of the XFROG signal beam has the form

$$E_{sig}^{SFG}(t,\tau) \sim E(t)\, E_{ref}(t-\tau) \tag{3.20}$$

for SFG, while

$$E_{sig}^{DFG}(t,\tau) \sim E(t)\, E_{ref}^{*}(t-\tau) \tag{3.21}$$

for DFG if the unknown pulse has a higher carrier frequency than the reference pulse. Here $E(t)$ is the unknown electric field, while $E_{ref}(t-\tau)$ indicates the reference one. The corresponding carrier frequency of the correlation signal is

$$\omega_0^{SFG} = \omega + \omega_{ref}$$

and

$$\omega_0^{DFG} = \omega - \omega_{ref}\,,$$

respectively. The XFROG trace, according to Eq. 3.7, is the squared magnitude of the spectrum of the cross-correlation signal recorded as a function of delay τ between the two pulses

$$I_{FROG}^{SFG}(\omega,\tau) \sim \left| \int_{-\infty}^{+\infty} E(t)\, E_r(t-\tau)\, e^{-i\omega t}\, dt \right|^2 . \tag{3.22}$$

Eq. 3.22 is relatives to SFG FROG. The corresponding equation for DFG XFROG can be obtained from a simple replacement of $E_r(t-\tau)$ with $E_r^*(t-\tau)$. (In analogous way it is possible to extrapolating the third-order XFROG processes).

XFROG is able to characterize very weak pulse because, according to Eq. (3.20), the XFROG signal field is proportional to the field of the reference pulse. A weak pulse produces a much weaker nonlinear signal in FROG, even with the most sensitive nonlinear optical process—second-harmonic generation (SHG). Indeed, according to Eq. 3.8, SHG signal strength is proportional to the square of the unknown pulse. Conversely,

in XFROG the same second-order nonlinear optical process (SFG or DFG), yields a nonlinear signal that is proportional to both the unknown pulse and the reference pulse, as shown in Eq. 3.20.

While XFROG has the usual trivial absolute-phase ambiguity, it lacks the translation ambiguity because the indipendent gate pulse acts as the time reference. XFROG also lacks the direction-of-time ambiguity because the trace is not necessary symmetrical with respect to the delay τ. A schematic diagram of an SFG/DFG XFROG apparatus is shown in Fig. (3.7).

An XFROG trace is also easier to interpret than a FROG trace. A FROG trace is produced by gating the pulse with itself. Both interacting pulses are, by definition, equally complicated. Although it is quite possible to read pulse information such as chirp directly from a FROG trace of a simple pulse, it is usually not straightforward with a complicated pulse. And, because the two pulses are the same, SHG-FROG and other even-order FROG techniques suffer from a direction-of-time ambiguity, by which a positive and a negative chirp cannot be differentiated. An XFROG trace, on the other hand, is produced by gating the unknown pulse, with a known reference or gate pulse. The produced trace is a true spectrogram. If the reference pulse is short and simple, as is almost always the case, the XFROG trace can simply be read as a plot of frequency versus time (a positively chirped pulse and a negatively chirped pulse have opposite slopes in their XFROG traces). Consequently, one often finds that the XFROG trace is very intuitive and easy to interpret, which makes it an ideal tool for the representation and analysis of complicated pulses.

XFROG is useful whenever an already measured reference pulse, that is shorter than the unknown pulse, is available. In this case, it is preferable to use this reference pulse to measure the unknown pulse, rather than its replica (FROG). Indeed, even if the reference pulse is not shorter, it is still usually preferable to use it to measure the unknown pulse. If the reference pulse is intense, then it yields higher efficiency in any non-linear optical process. This is especially helpful when the unknown pulse is weak enough that it does not yield sufficient signal strength using even the most sensitive FROG geometries, like SHG FROG. For example, UV pulses with energies of less than about a nJ are too weak to be measured using a third-order FROG technique, and SHG FROG is not available because SHG crystals absorb at the SH of such a puse ($\lesssim 190\,\mathrm{nm}$). Also, when measuring a very complex pulse of any energy, like the supercontinuum output pulse of a crystal fiber, gating it with a reference pulse that happens to be smooth will generate a trace that is easier to interpret. The need for a fairly strong reference pulse does not represent much of a limitation because such a pulse is in principle always available even when working with extremely weak pulses. Indeed, in most cases, weak pulses are the result of a linear or non-linear optical process, which involves at least one input pulse that is much stronger and therefore can be characterized by a standard FROG technique. For instance, supercontinuum pulses may be weak, difficult to collimate and incoherent, but pulse that generate them are usually from a Ti:Sapphire laser, in the near IR. Thus the near IR pulses are available to serve as a reference pulse, and XFROG can measure these otherwise difficult-to-measure pulses.

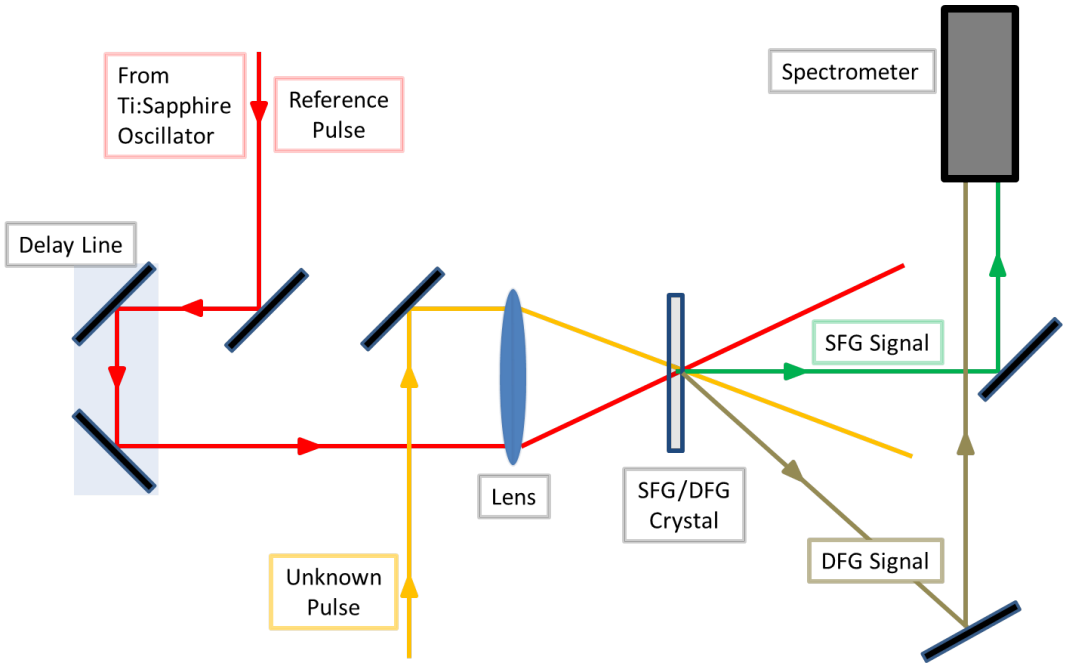

Figure 3.7: SFG and DFG XFROG. In this geometry: a known pulse generated from the laser source is used as the reference pulse; a pulse coming from an experiment is the unknown pulse; the reference pulse goes inside the delay line; the two pulses are focused in a SFG/DFG crystal, so that both their foci are spatially overlapped inside the mean; the spectrometer measure the intensity in function of the frequency; varying the delay of the gate field one measure the intensity in function of the delay; depending on the crystal type and on the position of the mirror that collect the signal, one gets a SFG or a DFG FROG trace.

If the unknown pulse spectrum is contained within that of the reference pulse, an alternative approach is spectral interferometry which is a linear optical technique. However, a key requirement to use spectral interferometry is that the reference pulse has to have equal or larger bandwidth than the pulse we want to measure, since spectral fringes only appear in the overlapped region of the spectra of the two pulses. For instance, spectral interferometry cannot be used to measure the microstructure-fiber supercontinuum. Indeed, the continuum is so broadband that no reference pulse is available for its measurement. Although XFROG does involve a non-linear optical interaction, and hence is less sensitive than spectral interferometry, it is much more versatile and easier to perform. In fact, XFROG requires no spectral overlap between the reference and unknown pulses and it does not need to satisfying interferometric alignment accuracy.

Summarizing:

- Advantages of XFROG are the generation of a fairly intuitive XFROG traces (also for complicated unknown puses), the absence of cross polarizers, the sensibility (given by a relatively strong reference pulse), the availability in different spectral regions, the absence of scattering (since the signal frequency is different from the input frequencies).

- Disadvantages of the XFROG are the need for a relatively strong reference pulse already characterized through FROG technique, the limitation of the maximum length of the crystal (because of group-velocity mismatch).
- Useful for measuring supercontinuum and UV pulses (since can be very sensitive and available in several spectral regions).

3.4.7 Summary

In Tab. 3.1 are reported the main characteristics of the various FROG beam geometries.

Geometry	PG	SD	TG	SHG	THG	X
Non-linearity	$\chi^{(3)}$	$\chi^{(3)}$	$\chi^{(3)}$	$\chi^{(2)}$	$\chi^{(3)}$	$\chi^{(2)}$
Sensitivity (single-shot)	$\sim 1\,\mu$J	$\sim 10\,\mu$J	$\sim 0.1\,\mu$J	$\sim 0.01\,\mu$J	$\sim 0.03\,\mu$J	
Sensitivity (multi-shot)	~ 100 nJ	~ 1000 nJ	~ 10 nJ	~ 0.001 nJ	~ 3 nJ	
Advantages	Intuitive traces; Automatic phase matching.	Intuitive traces.	Background free; Sensitive; Intuitive traces.	Very Sensitive.	Sensitive; Very large bandwidth.	Very Sensitive; Different spectral regions.
Disadvantages	Requires polarizers.	Requires thin medium; Not phase matched.	Three beams.	Unintuitive traces; Short-λ range.	Unintuitive traces; Very short-λ range.	Unintuitive traces; Requires reference beam.
Ambiguities	None known.	None known.	None known.	Direction of time; Rel. phase of multiple pulses: $\varphi, \varphi+\pi$.	Relative phase of multiple pulses: $\varphi, \varphi\pm 2\pi/3$.	Relative phase of multiple pulses: $\varphi, \varphi+\pi$.

Table 3.1: Brief summary of the characteristics of the various FROG beam geometries. Single-shot and multi-shot sensitivity values are very rough and assume 800 nm, 100 fs pulses from a regeneratively amplified or unamplified Ti:Sapphire oscillator, respectively, using a weak focus to about 100 μm in the nonlinear medium. Tighter focus (10 μm) is assumed in THG FROG because the nonlinearity assumed for this table is a surface effect, and the resulting decrease in Rayleigh range results in no loss of signal.

Beyond these traditional versions, other FROG geometries have been developed,

which can be applied even to very short pulses (where strong effects of group velocity mismatch in the non-linear crystal are removed through angle dithering of the crystal - Chap. 5) or to fairy long pulses (where a high spectrometer resolution is required). A particularly compact setup is achieved with the GRENOUILLE geometry, which has no moving parts and even allows the measurements of additional features such as spatial chirps. Cascaded $\chi^{(2)}$ effects can be used to mimic the functional form of self-diffraction of third-harmonic generation and may have longer effective non-linear coefficients $\chi^{(3)}_{eff}$ than usual third-order non-linearities. However, they suffer from a more complicated alignment procedure.

Chapter 4

SHG FROG in microscopy

In this Chapter we will reconsider the SHG FROG technique (treated in Chap. 3 - Sec. 4.4) in the case of a collinear geometry, then we will discuss the possibility of its application to the measurement of the pump pulses in a pump & probe technique coupled to a microscopy system. At last there will be a section dedicated to the testing of the SHG FROG phase-retrieval algorithm by means of some numerical simulations.

4.1 Collinear SHG FROG [19]

Ultrashort-pulse lasers are commonly used for multiphoton microscopy. The performance optimization of such systems requires careful characterization of the pulses at the tight focus of the microscope objective. Determining the optimum exposure conditions, i.e. those that provide the best combination of image resolution, contrast, and specimen viability, requires an accurate picture of the field $E(t)$ at focus. Thus a method for accurately determining the pulse intensity $I(t)$ and phase $\varphi(t)$ at the focus produced by a microscope objective is vital.

This problem can be solved using a collinear geometry in frequency-resolved optical gating that exploits type II second-harmonic generation and that allows the full numerical aperture (N.A.) of the microscope objective to be used. This technique has been demonstrated by [19] through the measure of intensity and phase of a 22-fs pulse focused by a 20×, 0.4-N.A. air objective in a potassium-dihydrogen-phosphate (KDP) crystal.

Usually FROG systems are based on non-collinear geometries (such the one of Fig. (3.1)). Anyway, for the case of pulses focused by an objective with a high N.A., a collinear geometry allows to exploit the full N.A. of the objective. This permits the production of the tightest focus possible and, subsequently, the greatest intensity and the highest spatial resolution. Thus, for multiphoton microscopy, it is desirable to use a collinear FROG geometry for measurements at the focus of high-N.A. objectives.

The use of a collinear geometry requires the type II phase-matching rather than the type I. This is due to the fact that in type II phase-matching the signal field $E_s(t, \tau)$ is background free. In other words, in a type II phase-matching collinear geometry an input beam is an ordinary wave $E_o(t)$, while the other one is an extraordinary wave

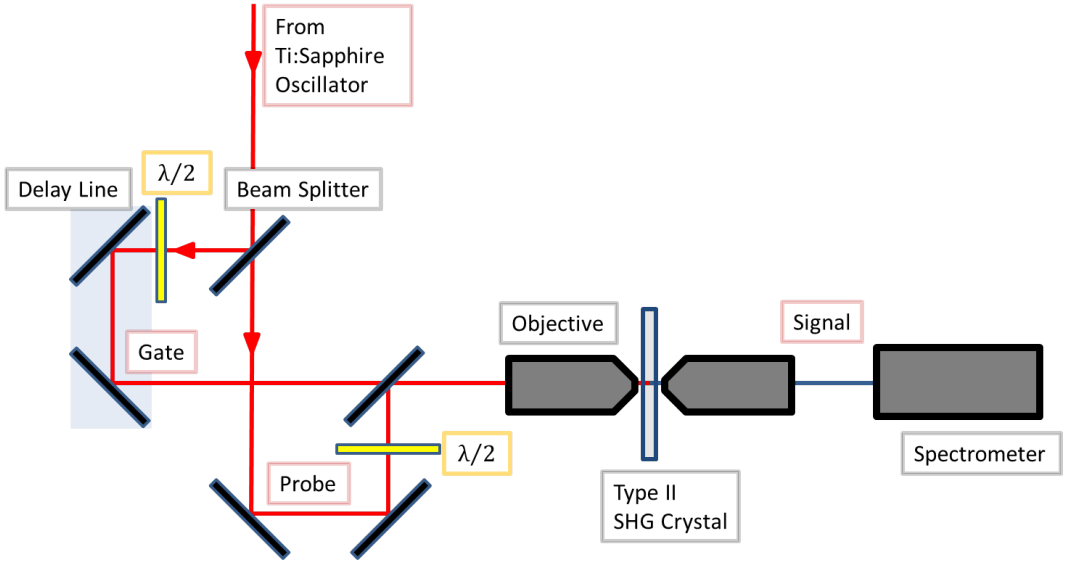

Figure 4.1: type II SHG FROG. In this geometry: a pulsed laser beam is duplicated through a beam-splitter; the pulsed beam that continue below is called probe; the pulsed beam that go inside the delay line is called gate; a 90° polarization rotation between the two arms is induced placing a $\lambda/2$ wave plate in each arm; the two beams are made collinear and lead into the first microscope objective; the two collinear pulses are focused in a second-harmonic crystal (under type II phase-matching condition), so that both their foci are spatially overlapped inside the mean; the spectrometer measure the intensity in function of the frequency; varying the delay of the gate field one measure the intensity in function of the delay.

$E_e(t)$. This provides that the signal beam must be generated by the combination of the ordinary and extraordinary waves $E_s(t,\tau) \sim E_o(t)\, E_e(t-\tau)$, and by this only. On the other hand, a hypothetical collinear geometry based on type I phase-matching is not background free. In a type I phase-matching collinear geometry there are two ordinary waves: wave-1 with field $E_{1o}(t)$ and wave-2 with $E_{2o}(t)$. This situation produces a signal beam that is the result of the combination of wave-1 and wave-2, but also of the auto-interaction of wave-1 and wave-2 with themselves. Therefore the signal field will be an extraordinary wave, with form $E_s(t,\tau) \sim E_{1o}(t)\, E_{2o}(t-\tau) + \alpha \left[E_{1o}^2(t) + E_{2o}^2(t-\tau)\right]$, and this will overlap tangles the things up.

The experimental setup for type II SHG FROG is similar to the one proposed for SHG FROG of Fig. (3.1), except that, as shown in Fig. (4.1), the beams are collinear, and there is a 90° polarization rotation between the two arms of the FROG interferometer. Type II SHG FROG also uses type II phase matching instead of type I phase matching.

Type II SHG FROG has several noteworthy advantages.

- The signal field $E_s(t,\tau)$ for type II SHG FROG is identical to that for SHG FROG, that is, according to Eq. (3.8)

$$E_s^{SGH}(t,\tau) \sim E(t)\, E(t-\tau)\,. \tag{4.1}$$

Thereby the traces $I_{FROG}(\omega,\tau)$ for type II SHG FROG are identical to the SHG FROG traces, with mathematical form given by Eq. (3.7)

$$I_{FROG}^{SGH}(\omega,\tau) \sim \left| \int_{-\infty}^{+\infty} E(t)\, E(t-\tau)\, e^{-i\omega t}\, dt \right|^2 . \tag{4.2}$$

For this reason the already-existing SHG FROG algorithms can be used to retrieve the intensity and phase for the type II SHG FROG case.

- Current laser systems routinely produce pulses shorter than 30 fs, and several research groups have produced pulse widths of 10 fs or less. These pulses are only a few optical cycles long, but careful control of dispersion, group delay as a function of radius in the objective, and other system parameters could potentially allow few-cycle pulses to be focused by microscope objectives. For all non-collinear geometries, the finite crossing angle of the beams produces temporal blurring. For asymmetric FROG geometries, the finite thickness of the nonlinear medium also produces geometrical distortions that produce temporal blurring. The use of a collinear geometry eliminates these problems.

- In a type II crystal the two different polarizations propagate along different optical axes, and the different propagation velocities along those axes produce a temporal walk-off in the type II crystal between the two polarizations. For a 50 μm-thick type II KDP crystal, the temporal walk-off is approximately 8 fs. Such a large walk-off would badly distort the FROG signal for pulses of <50 fs. If the confocal parameter is much shorter than the crystal thickness, however, the effective interaction may be much shorter, which greatly reduces the temporal walk-off. The blurring that is due to the walk-off will usually be negligible for multiphoton microscopy when high-N.A. objectives are used. Furthermore the short interaction region also increases the effective phase-matching bandwidth. Alternatively, shorter crystals could be used.

4.2 Collinear SHG FROG for pump characterization

A collinear type II SHG FROG can be easily applied to the reference setup of Fig. (2.3), as shown in Fig. (4.2). Without taking off any optical piece of the reference setup, it is sufficient to add a SHG crystal at the microscope focus; a 'probe-gate generator system' before the microscope and a spectrometer immediately after it.

4.3 Numerical simulations for SHG FROG [18]

The FROG algorithm is what makes FROG the powerful technique that it is. It takes a measured trace and retrieves the pulse intensity and phase versus time and frequency. This section is about the numerical testing of the SHG FROG phase-retrieval algorithm. To this purpose we used a FROG code written in Matlab which is available on the

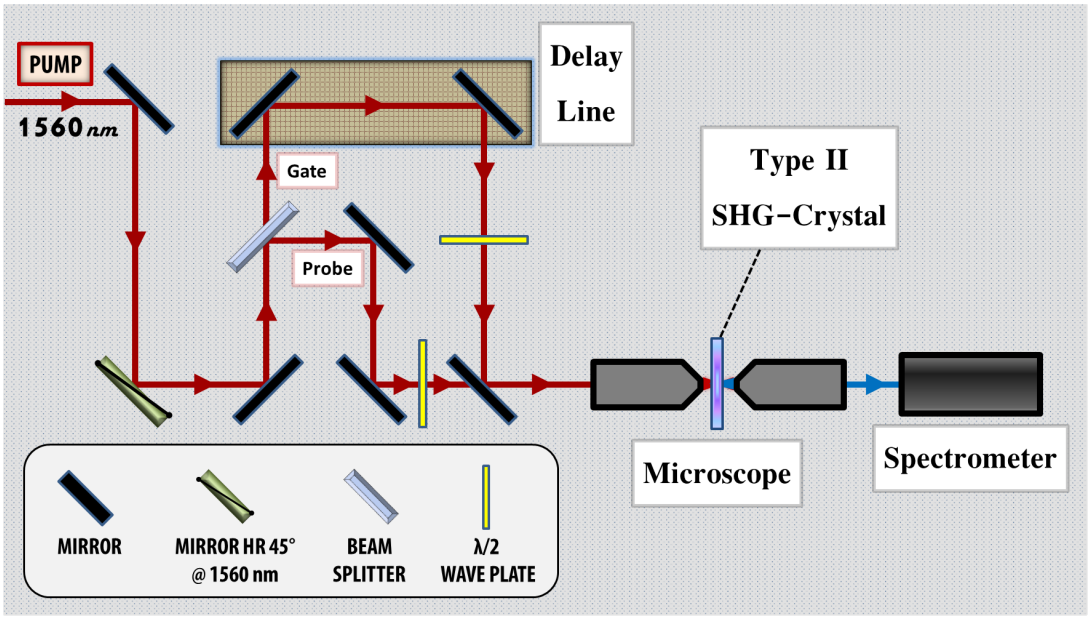

Figure 4.2: Type II SHG FROG applied to our reference setup for the pump pulse characterization at the focus of the microscope objective. To work with this geometry the probe laser (@ 780 nm) must be turn off. Only the pump laser (@ 1560 nm) is required. The path of the pump pulse immediately before the microscope is modified to produce a probe and a gate pulse (some mirrors and a delay line should be placed in loco). Both the pulses go through a half-wave plate so that the probe pulse become an ordinary wave, while the gate pulse results in an extraordinary wave. The two pulses are made collinear and lead to the microscope. A SHG crystal must be placed in the focal zone, in the position where an hypothetical sample would be placed. Finally, immediately after the microscope, a spectrometer is set. As always, the spectrometer measure the intensity in function of the frequency; varying the delay of the gate field one measure the intensity in function of the delay.

Trebino group's web site "`http://frog.gatech.edu/code.html`". This code aims to retrieve a pulse intensity and phase from its FROG trace.

With the FROG code ready, typing 'frogger' in the Command Window of Matlab will open a graphical user interface (GUI). This FROG GUI allows an intuitive use of the FROG phase-retrieval algorithm. Two main input are required: the specification of the FROG geometry and the FROG trace $I_{FROG}(\omega, \tau)$. As regards the geometry, we are interested in the second-harmonic generation FROG (SHG FROG). As far as concerns the second input, the FROG trace, we used a numerically generated trace. This was achieved writing a Matlab program.

The program starts with the definition of the probe electric field in time domain $E(t)$ as a Matlab vector. Through this information are generated the Fourier transform of the probe in frequency domain $\tilde{E}(\nu)$, which is another Matlab vector, and the SHG FROG trace in frequency-delay domain $I^{SHG}_{FROG}(\nu, \tau)$, that is a Matlab matrix of dimensions $2^N \times 2^N$ ($N = 1, 2, 3...$). Due to practical reasons we used the frequency ν here, defined

as $\nu = \omega/(2\pi)$. According to Eqs. (3.1) and (3.3) the probe electric field is determined by the temporal intensity $I(t)$ and phase $\varphi(t)$, while its Fourier transform is defined by the spectral intensity $\tilde{I}(\nu)$ and phase $\tilde{\varphi}(\nu)$

$$E(t) = \sqrt{I(t)}\, \exp(i2\pi\nu_0 t - i\varphi(t))\,,$$

$$\tilde{E}(\nu) = \sqrt{\tilde{I}(\nu - \nu_0)}\, \exp(i\tilde{\varphi}(\nu - \nu_0))\,.$$

The SHG FROG trace has been constructed following Eq. (3.18), here reported

$$I^{SHG}_{FROG}(\nu, \tau) \sim \left| \int_{-\infty}^{+\infty} E(t)\, E(t-\tau)\, e^{-i2\pi\nu t}\, dt \right|^2 .$$

This SHG FROG trace $I^{SHG}_{FROG}(\nu, \tau)$ has been used as the second input of the FROG GUI.

Running the algorithm (by typing 'Run' on the FROG GUI) and waiting for the completion of several hundreds cycles - see Fig. (3.2) for the diagram of a cycle - the probe intensity and phase are retrieved in both the domain of time and frequency. Further, at the end of every cycle, a "retrieved trace" from the retrieved pulse is computed. This is important because, if the measured and retrieved traces agree, then the measurement is a good one, free of systematic error. This confirmation of a measurement is unique to FROG, and other techniques without it have often been found to yield wildly incorrect measurements.

To test the algorithm we have compared those retrieved intensities and phases with the ones used in the production of the trace $I^{SHG}_{FROG}(\nu, \tau)$.

Below we present the results of these numerical simulations in some simple cases. In every case there is a good agreement between the original an the retrieved data. In some cases the retrieved phase differs from the original one, but the variations are always negligible in the zone where the field modulus is non-zero and important only where it is null. Also, differences which are multiples of π are not physically relevant. The main problem one can run into using the algorithm in the SHG case, is the time direction ambiguity as shown in Figs. (4.8) and (4.9), or in Figs. (4.15) and (4.16). These two couples of figures have been obtained using the button 'Flip Time' on the FROG GUI. Both the retrieved fields in each couple have the same right to be the correct result because of the time ambiguity. Nevertheless, this problem can be experimentally solved as stated in Chap. 3 - Sec. 4.4.

4.3.1 Gaussian profile, constant phase

In the first case, we have chosen a probe electric field defined by

$$E(t) = e^{-t^2/a^2} e^{i2\pi\nu_0 t}\,,$$

where $a = 10^{-14}\,\mathrm{s}$ and $\nu_0 = 3.75 \cdot 10^{14}\,\mathrm{Hz}$ (which corresponds to 800 nm). The field modulus has a Gaussian profile $|E(t)| = e^{-t^2/a^2}$, while the phase is zero $\varphi(t) = 0$. The

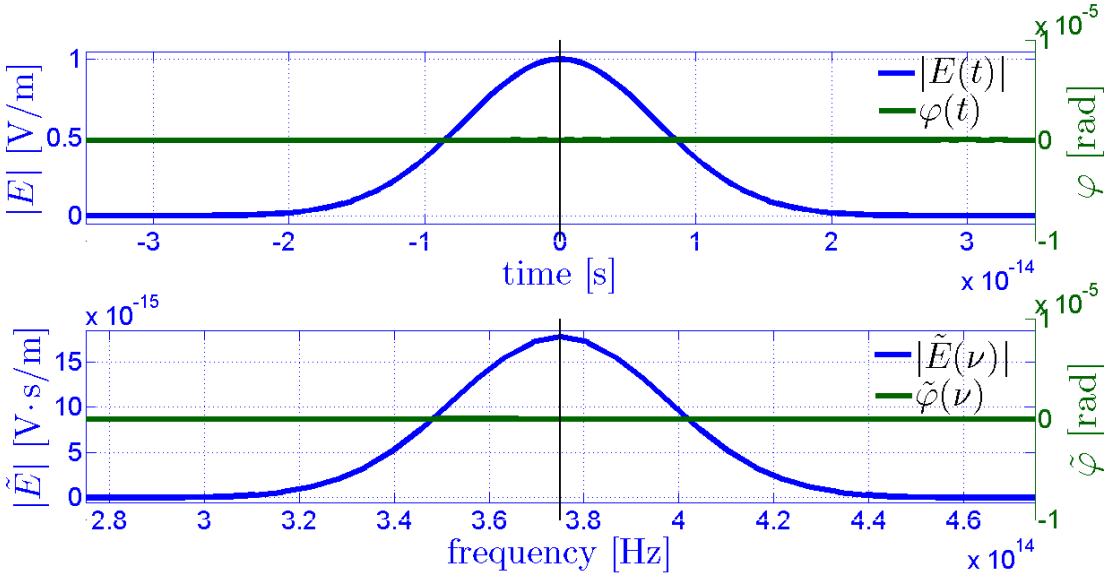

Figure 4.3: At the top is reported the graphic modulus $|E(t)|$ and phase $\varphi(t)$ of the probe electric field; at the bottom is shown the graphic of the modulus $|\tilde{E}(\nu)|$ and phase $\tilde{\varphi}(\nu)$ of the probe electric field Fourier transform.

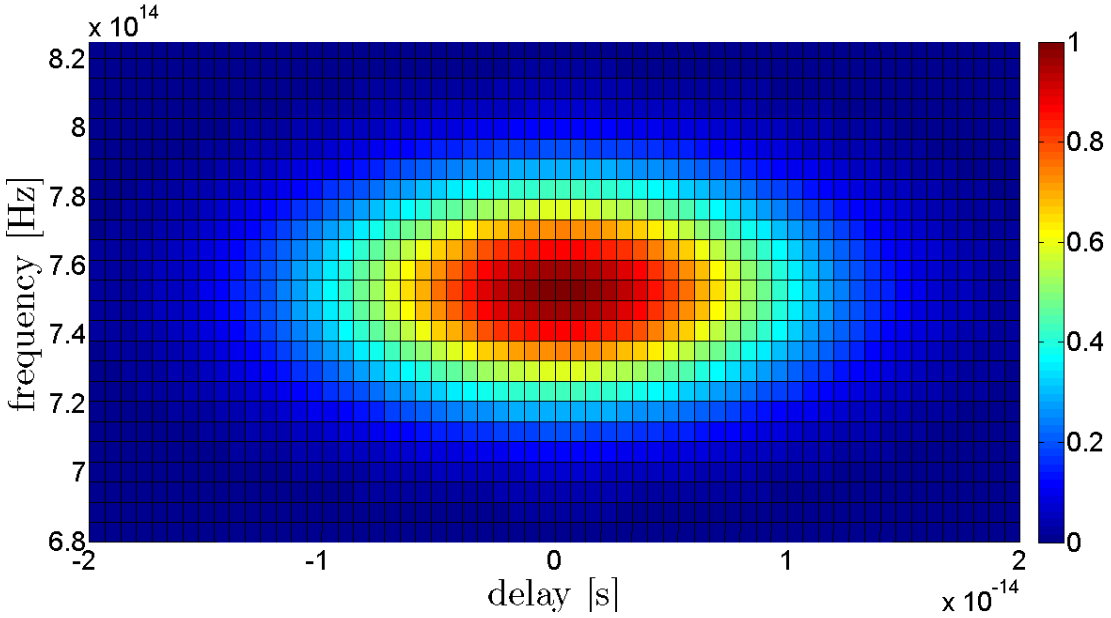

Figure 4.4: Bird's-eye view of the graphic of $I^{SHG}_{FROG}(\nu, \tau)$ versus delay τ and frequency ν.

probe field modulus and phase are both reported in the top graphic of Fig. (4.3), while in the bottom graphic are shown the Fourier transform probe field modulus and phase.

In Fig. (4.4) is shown the SHG FROG trace generated from the probe electric field.

Finally, in Fig. (4.5) are presented 4 graphics where the originals intensities and phases are compared with the retrieved ones.

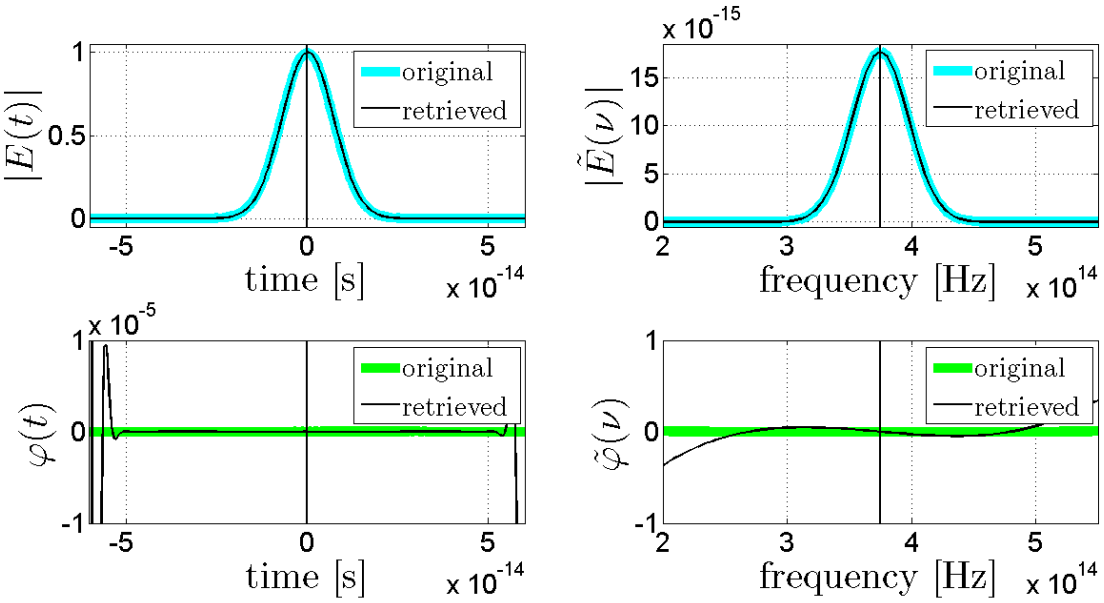

Figure 4.5: Comparison between the original probe electric field and the retrieved one. At the top-left side there is the graphic of the modulus of the field $|E(t)|$; at the bottom-left side of the phase of the field $\varphi(t)$; at the top-right side of the modulus of the FT of the field $|\tilde{E}(\nu)|$; at the bottom-right side the phase of the FT of the field $\tilde{\varphi}(\nu)$.

4.3.2 Gaussian profile, square phase

In the second case, we have chosen a probe electric field defined by

$$E(t) = e^{-t^2/a^2} e^{i2\pi\nu_0 t} e^{it^2/b^2} ,$$

that is the case of a negative linearly chirped pulse with instantaneous frequency $\omega(t) = \omega(0) - 2t/b^2$ (according to Eq. 3.2). Here $a = b = 10^{-14}$ s and $\nu_0 = 3.75 \cdot 10^{14}$ Hz (which corresponds to 800 nm). The field modulus has a Gaussian profile $|E(t)| = e^{-t^2/a^2}$, while the phase is quadratic in time $\varphi(t) = t^2/b^2$. The probe field modulus and phase are both reported in the top graphic of Fig. (4.6), while in the bottom graphic are shown the Fourier transform probe field modulus and phase.

In Fig. (4.7) is shown the SHG FROG trace generated from the probe electric field.

In Fig. (4.8) are presented 4 graphics where the originals intensities and phases are compared with the retrieved ones.

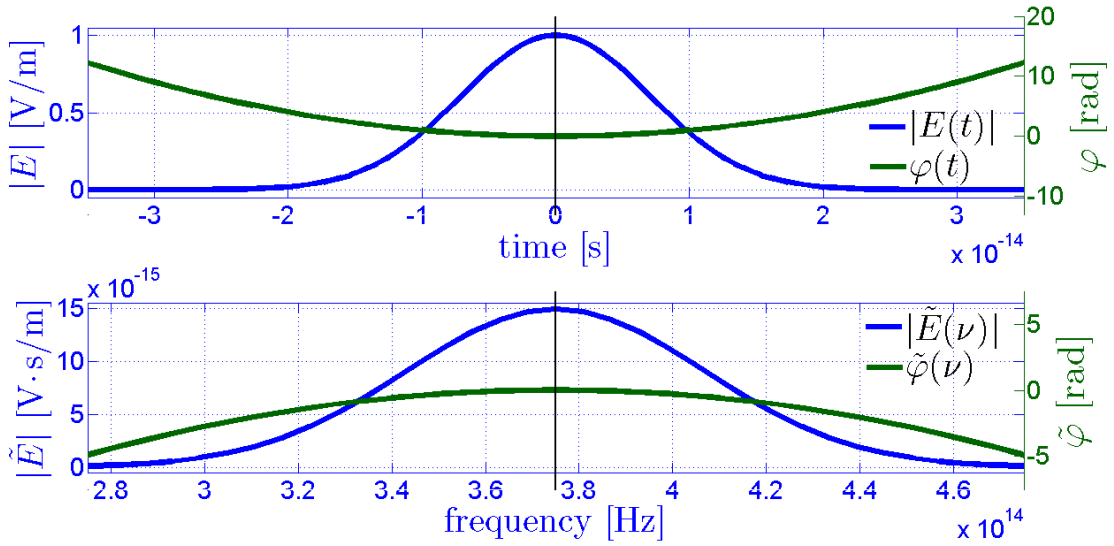

Figure 4.6: At the top is reported the graphic modulus $|E(t)|$ and phase $\varphi(t)$ of the probe electric field; at the bottom is shown the graphic of the modulus $|\tilde{E}(\nu)|$ and phase $\tilde{\varphi}(\nu)$ of the probe electric field Fourier transform.

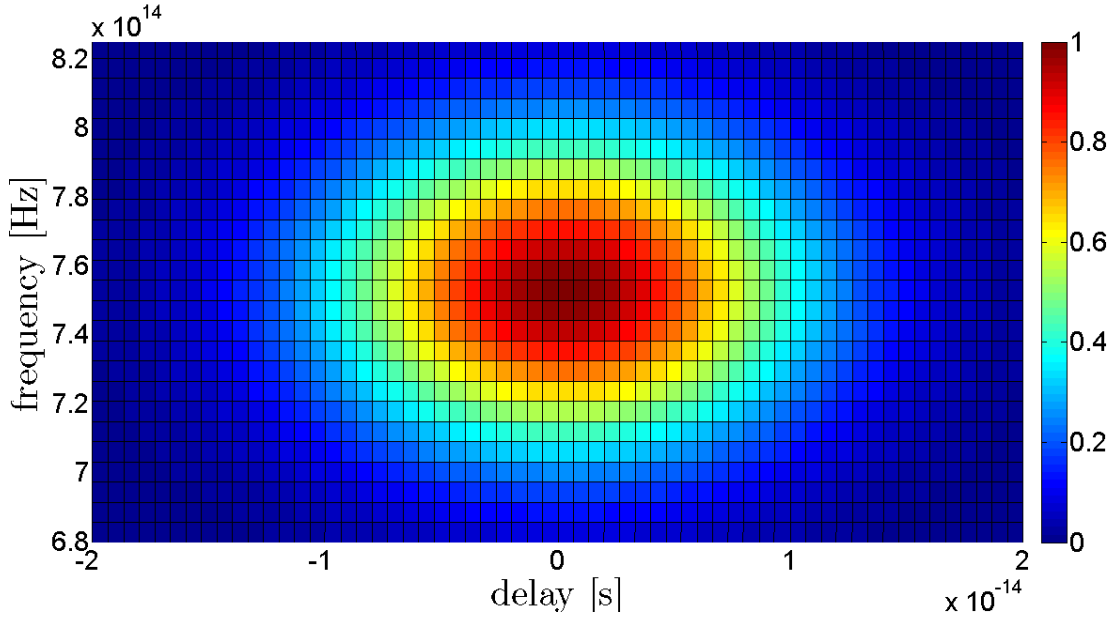

Figure 4.7: Bird's-eye view of the graphic of $I^{SHG}_{FROG}(\nu, \tau)$ versus delay τ and frequency ν.

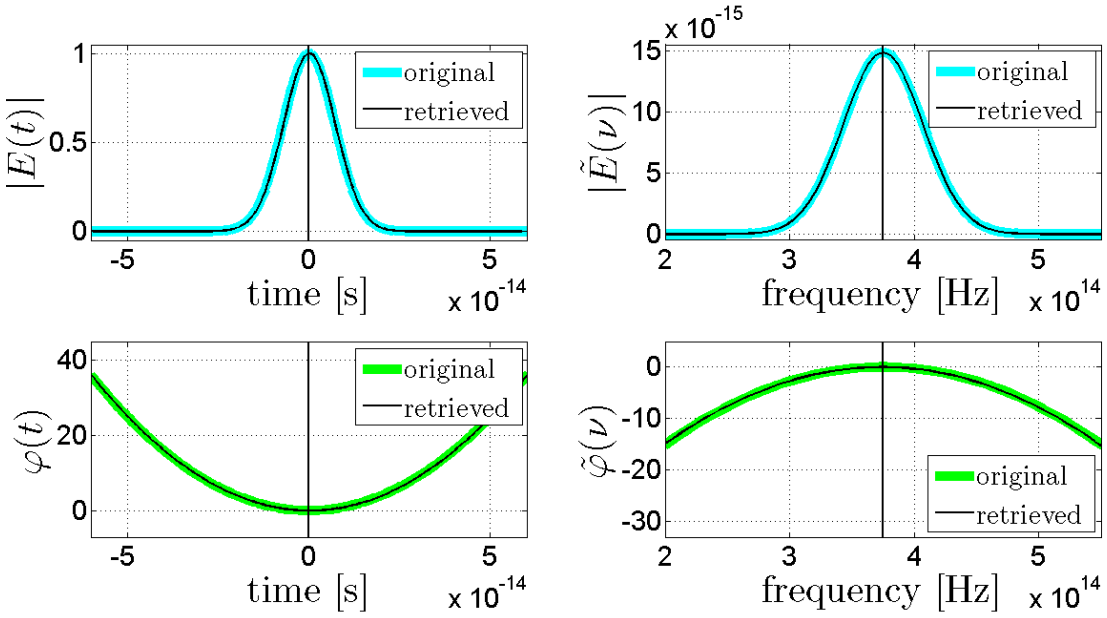

Figure 4.8: Comparison between the original probe electric field and the retrieved one. At the top-left side there is the graphic of the modulus of the field $|E(t)|$; at the bottom-left side of the phase of the field $\varphi(t)$; at the top-right side of the modulus of the FT of the field $|\tilde{E}(\nu)|$; at the bottom-right side the phase of the FT of the field $\tilde{\varphi}(\nu)$.

Since we are using the SHG FROG, the time direction ambiguity does not allow to discern between negative or positive chirp. The results obtained flipping the time axis are shown in Fig. (4.9).

4.3.3 Gaussian profile, cubic phase

In the third case, we have chosen a probe electric field defined by

$$E(t) = e^{-t^2/a^2} e^{i2\pi\nu_0 t} e^{it^3/b^3} ,$$

which is the case of a pulse with instantaneous frequency $\omega(t) = \omega(0) - 3t^2/b^3$ (according to Eq. 3.2). Here $a = b = 10^{-14}$ s and $\nu_0 = 3.75 \cdot 10^{14}$ Hz (which corresponds to 800 nm). As always the field modulus has a Gaussian profile $|E(t)| = e^{-t^2/a^2}$, while the phase is cubic in time $\varphi(t) = t^3/b^3$. The probe field modulus and phase are both reported in the top graphic of Fig. (4.6), while in the bottom graphic are shown the Fourier transform probe field modulus and phase.

In Fig. (4.11) is shown the SHG FROG trace generated from the probe electric field.

Finally, in Fig. (4.12) are presented 4 graphics where the originals intensities and phases are compared with the retrieved ones.

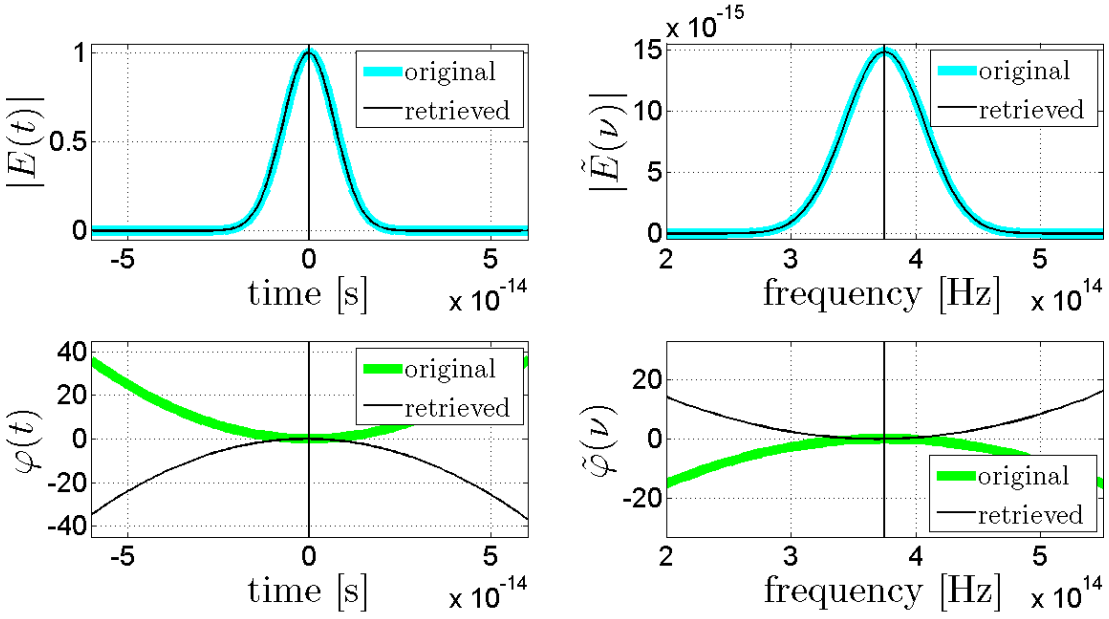

Figure 4.9: Comparison between the original probe electric field and the retrieved one. The direction of time has been reversed in respect to the case of Fig. (4.8) to illustrate the effects of the time ambiguity. At the top-left side there is the graphic of the modulus of the field $|E(t)|$; at the bottom-left side of the phase of the field $\varphi(t)$; at the top-right side of the modulus of the FT of the field $|\tilde{E}(\nu)|$; at the bottom-right side the phase of the FT of the field $\tilde{\varphi}(\nu)$.

4.3.4 Double Gaussian profile, constant phase

For the last case, we have chosen a probe electric field defined by

$$E(t) = \left(e^{-t^2/a^2} + \frac{1}{2}\, e^{-(t-t_0)^2/a^2} \right) e^{i2\pi\nu_0 t}\,,$$

where $a = 3.16 \cdot 10^{-15}\,\mathrm{s}$, $t_0 = 1.5 \cdot 10^{-14}\,\mathrm{s}$ and $\nu_0 = 3.75 \cdot 10^{14}\,\mathrm{Hz}$ (which corresponds to 800 nm). The field modulus is given by the sum of the two Gaussian profiles $|E(t)| = e^{-t^2/a^2} + 0.5\, e^{-(t-t_0)^2/a^2}$, while the phase is zero $\varphi(t) = 0$. The probe field modulus and phase are both reported in the top graphic of Fig. (4.13), while in the bottom graphic are shown the Fourier transform probe field modulus and phase.

In Fig. (4.14) is shown the SHG FROG trace generated from the probe electric field.

In Fig. (4.15) are presented 4 graphics where the originals intensities and phases are compared with the retrieved ones.

Since we are using the SHG FROG, the time direction ambiguity does not allow to understand the disposition of the two Gaussian peaks. The results obtained flipping the time axis are shown in Fig. (4.16).

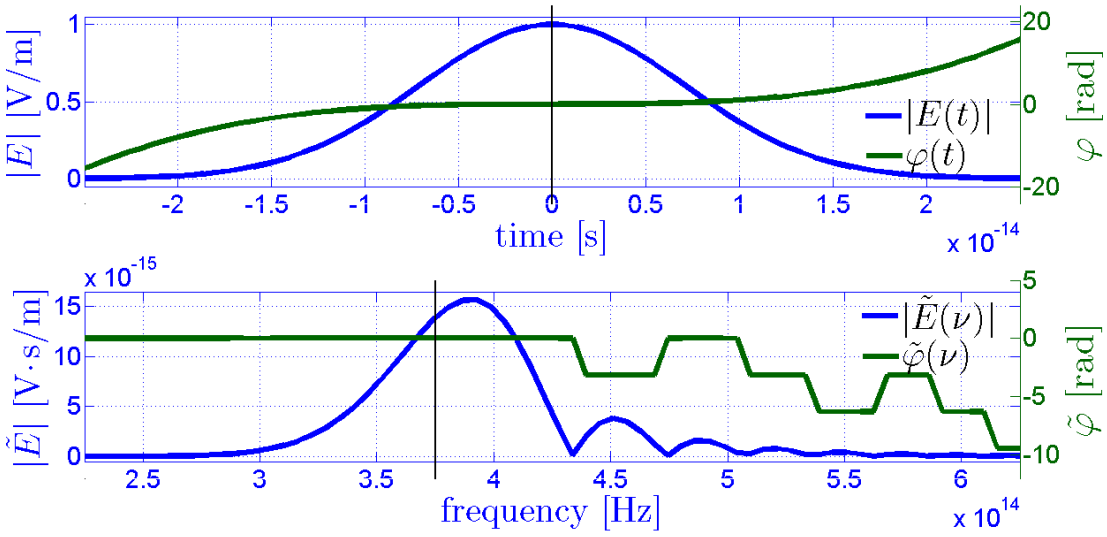

Figure 4.10: At the top is reported the graphic modulus $|E(t)|$ and phase $\varphi(t)$ of the probe electric field; at the bottom is shown the graphic of the modulus $|\tilde{E}(\nu)|$ and phase $\tilde{\varphi}(\nu)$ of the probe electric field Fourier transform.

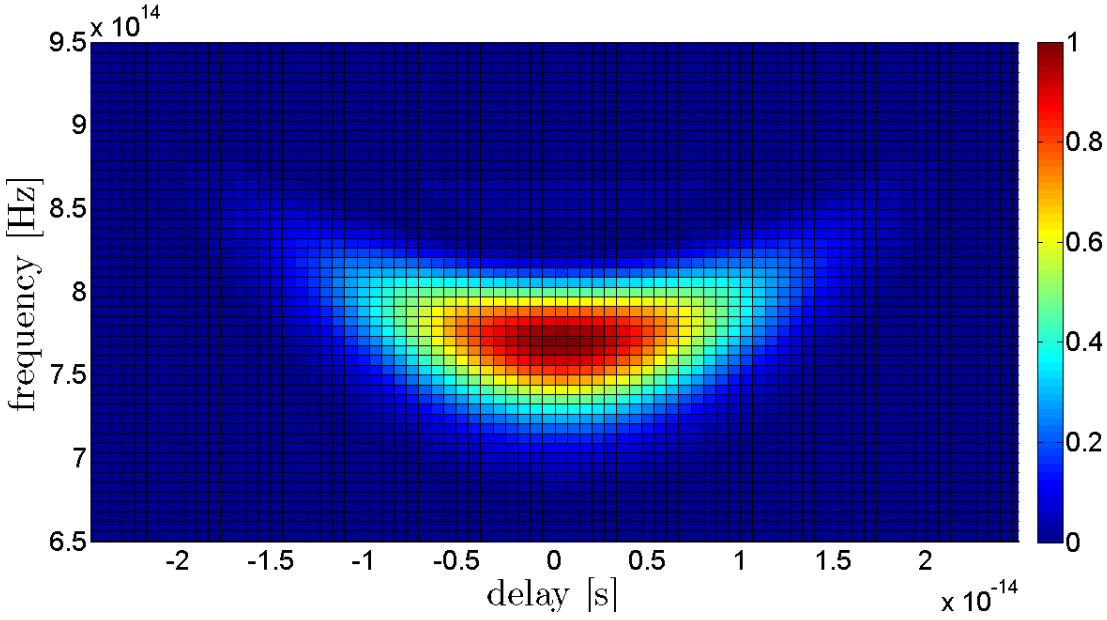

Figure 4.11: Bird's-eye view of the graphic of $I^{SHG}_{FROG}(\nu, \tau)$ versus delay τ and frequency ν.

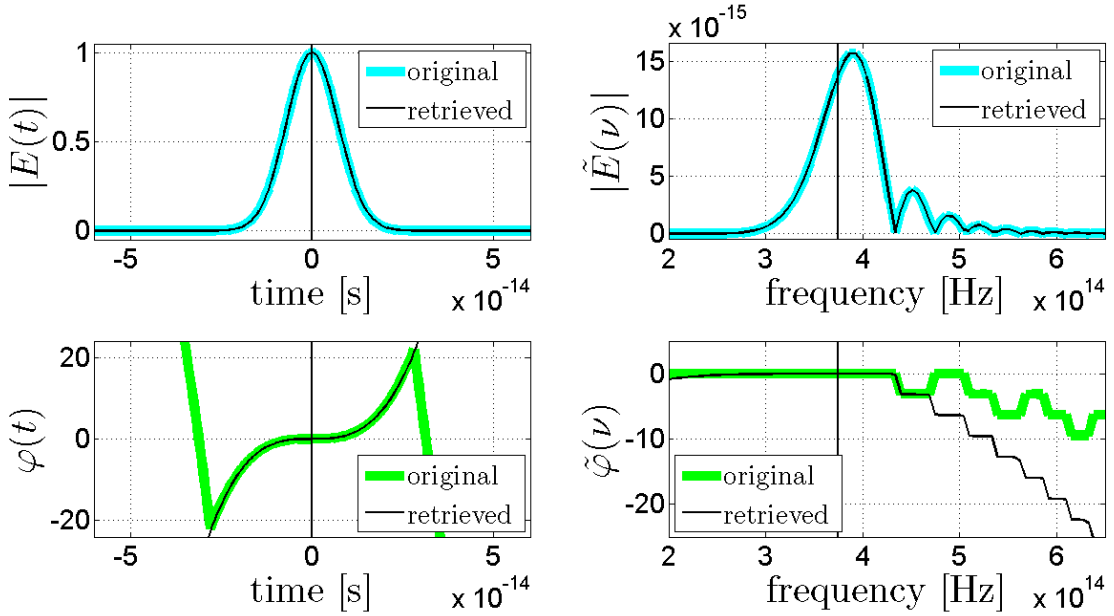

Figure 4.12: Comparison between the original probe electric field and the retrieved one. At the top-left side there is the graphic of the modulus of the field $|E(t)|$; at the bottom-left side of the phase of the field $\varphi(t)$; at the top-right side of the modulus of the FT of the field $|\tilde{E}(\nu)|$; at the bottom-right side the phase of the FT of the field $\tilde{\varphi}(\nu)$.

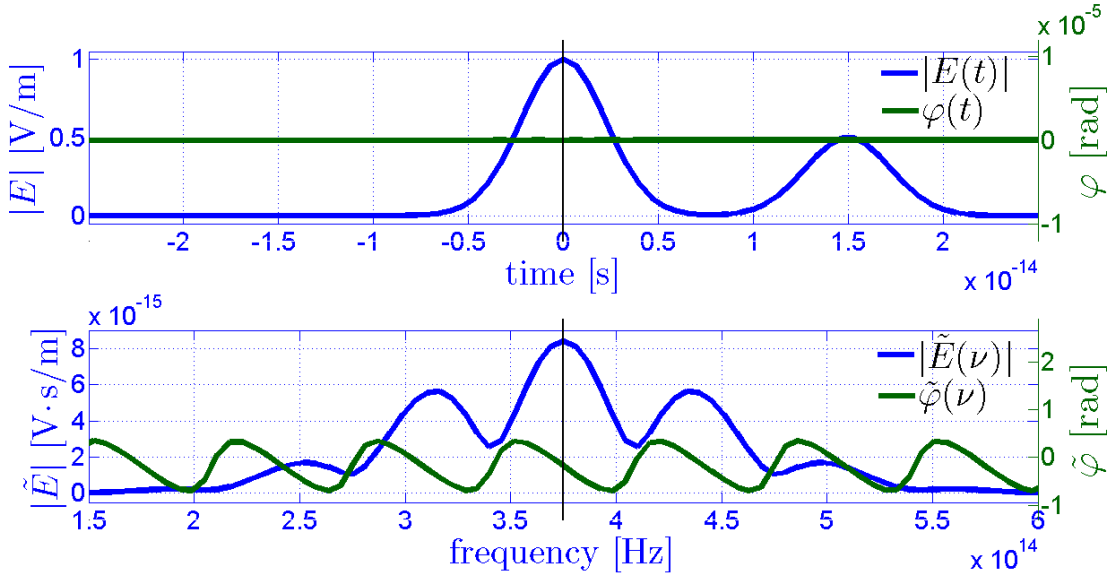

Figure 4.13: At the top is reported the graphic modulus $|E(t)|$ and phase $\varphi(t)$ of the probe electric field; at the bottom is shown the graphic of the modulus $|\tilde{E}(\nu)|$ and phase $\tilde{\varphi}(\nu)$ of the probe electric field Fourier transform.

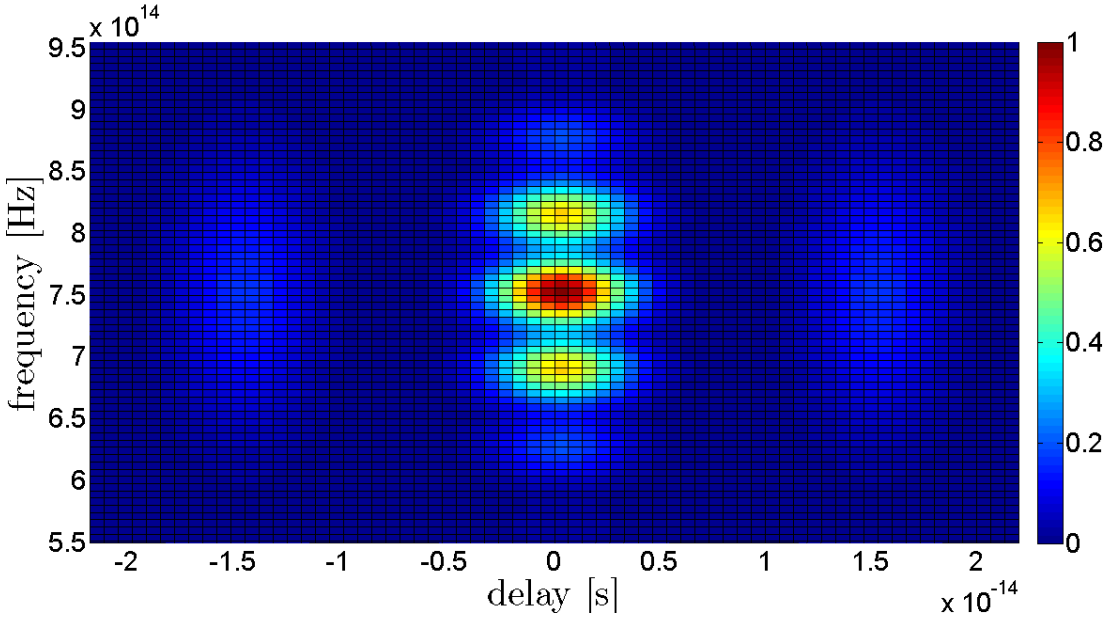

Figure 4.14: Bird's-eye view of the graphic of $I^{SHG}_{FROG}(\nu, \tau)$ versus delay τ and frequency ν.

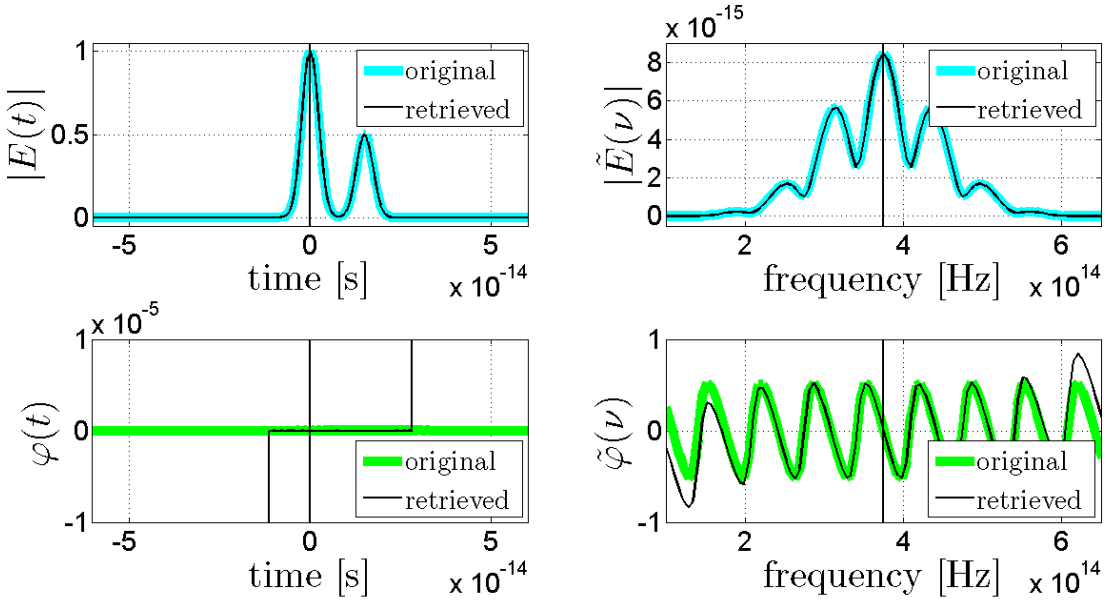

Figure 4.15: Comparison between the original probe electric field and the retrieved one. At the top-left side there is the graphic of the modulus of the field $|E(t)|$; at the bottom-left side of the phase of the field $\varphi(t)$; at the top-right side of the modulus of the FT of the field $|\tilde{E}(\nu)|$; at the bottom-right side the phase of the FT of the field $\tilde{\varphi}(\nu)$.

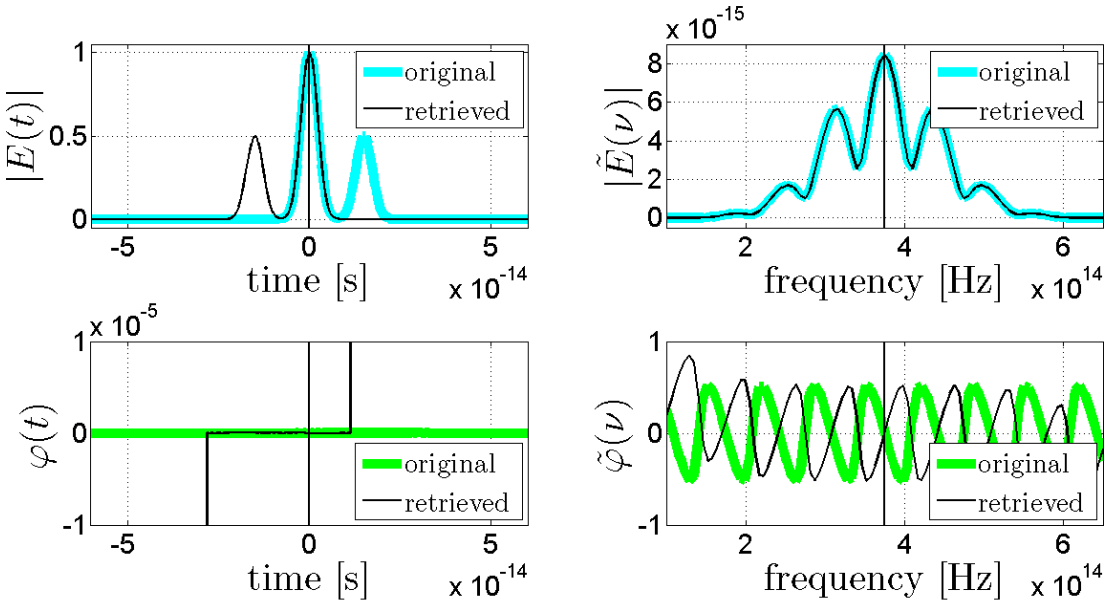

Figure 4.16: Comparison between the original probe electric field and the retrieved one. The direction of time has been reversed in respect to the case of Fig. (4.15) to illustrate the effects of the time ambiguity. At the top-left side there is the graphic of the modulus of the field $|E(t)|$; at the bottom-left side of the phase of the field $\varphi(t)$; at the top-right side of the modulus of the FT of the field $|\tilde{E}(\nu)|$; at the bottom-right side the phase of the FT of the field $\tilde{\varphi}(\nu)$.

Chapter 5

SFG XROG in supercontinuum

In this Chapter we will recover the XFROG technique (previously treated in Chap. 3 - Sec. 4.6) and we will discuss the possibility of its application to the measurement of the crystal-fiber continuum in a pump & probe technique coupled to a microscopy system.

5.1 Collinear SFG XFROG [17] [20] [21]

The generation of ultrabroadband supercontinuum (SC) spectra has been demonstrated by several groups by injecting high power pulses near the zero dispersion wavelength of photonic-crystal fibers (PCF). In particular, for SC generated with femtosecond pulse pumping, the dominant contribution to the long wavelength extension of the SC has been shown to be associated with soliton break up combined with the Raman self-frequency shift whilst an important contribution to the short-wavelength portion of the SC is due to the associated transfer of energy into the normal dispersion regime via the generation of non-solitonic dispersive wave radiation. The enhanced nonlinear response of PCFs permits their study in a regime not readily accessible with standard optical fibers. At the same time, however, it also leads to difficulties in accurately characterizing the complex temporal and spectral structure of the SC, and this has limited comparisons between theory and experiment to only relatively simple studies of the spectral properties via the positions of the observed Raman soliton peaks. However, the application of XFROG to SC characterization permits a complete intensity and phase characterisation of SC generated in PCF.

In the reference setup of Fig. (2.3) a pump and a SC probe pulse are used for multiphoton microscopy. The probe pulse, initially @ 780 nm, its used for broadband SC generation through a photonic-crystal fiber. On the other hand the pump pulse remains coherent @ 1560 nm and it can be characterized at the objective focus using the method illustrated in Chap. 4.

Since an unknown broadband SC pulse and a completely characterized pulse (that has much higher intensity) are available, the XFROG results in the most useful FROG variant. The microstructure-fiber supercontinuum is the most complicated pulse ever

generated. Requiring only an oscillator pump, its pulse energy is on the order of nJ, and its bandwidth is very broad. To use FROG to measure the continuum, an extremely thin SHG crystal has to be used, which would produce minuscule amount of signal. Although it's not entirely impossible, and may still be the only possible method to use in certain cases such as to measure a few-cycle continuum pulse after compression, using FROG to measure the microstructure fiber continuum will be very difficult. XFROG, in comparison, is a better choice. Specifically, here we are interested in the characterization of the SC probe pulse at the focus of the objective (where an hypothetical sample would be placed). A setup for multiphoton microscopy based on the SFG XFROG technique is schematically reported in Fig. (5.1).

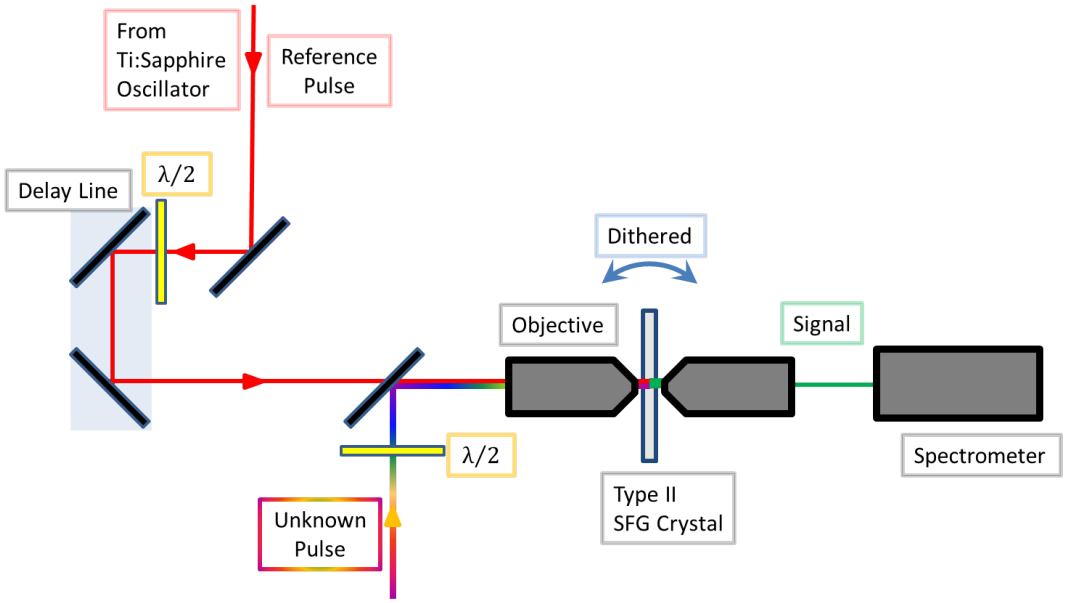

Figure 5.1: type II SFG XFROG. In this geometry: a known pulse generated from the laser source is used as the reference pulse; a pulse of output of the crystal fiber is the unknown pulse; the reference pulse goes inside the delay line; a 90° polarization rotation between the two arms is induced placing a $\lambda/2$ wave plate in each arm; the two beams are made collinear and lead into the first microscope objective; the two collinear pulses are focused in a sum-frequency-generation crystal (under type II phase-matching condition), so that both their foci are spatially overlapped inside the mean; the crystal is rapidly angle-dithered allowing for phase-matching at all wavelengths in the continuum; the spectrometer measure the intensity in function of the frequency; varying the delay of the reference field one measure the intensity in function of the delay.

As explained in Chap. 4 - Sec. 1, in the case of multiphoton microscopy, where the pulses are focused by an objective with a high N.A., a collinear geometry is required. Indeed this allows to exploit the full N.A. of the objective, while the mathematical form of the experimental trace remains identical to the non-collinear case. The use of a collinear geometry requires the type II phase-matching and, consequently, the introduction of a 90° polarization rotation between the pump and the probe pulses by the means of two

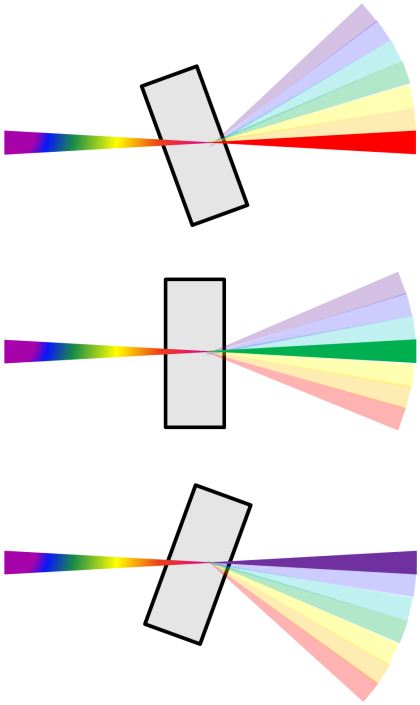

Figure 5.2: The effective bandwidth can be extended through angle-dithering. While a "thick" non-linear crystal may not phase-match the entire pulse at once, dithering the crystal can cover the full bandwidth of the pulse. Dithering much more quickly than the integration time of the measurement can increase the effective overall bandwidth of otherwise too-thick crystals.

$\lambda/2$ wave plates.

At the focus of the objective a non-linear crystal must be placed. Assuming that a SFG crystal is available, for instance a beta-barium-borate (BBO) crystal, the SFG XFROG technique can be exploited.

In according to Eq. 3.20, the electric field of the SFG XFROG signal beam has the form

$$E_{sig}^{SFG}(t,\tau) \sim E(t)\, E_{ref}(t-\tau)\,,$$

where $E(t)$ and $E_{ref}(t)$ are respectively referred to the unknown (SC probe) and to the reference (pump) pulses. The corresponding carrier frequency of the signal is given by

$$\omega_0^{SFG} = \omega + \omega_{ref}\,.$$

The SFG XFROG trace, recovering Eq. 3.22, is

$$I_{FROG}^{SFG}(\omega,\tau) \sim \left| \int_{-\infty}^{+\infty} E(t)\, E_r(t-\tau)\, e^{-i\omega t}\, dt \right|^2 .$$

For the SFG XFROG measurement, the SC probe pulse must be gated by the 1560 nm pump pulse in a BBO crystal, which has to be rapidly angle-dithered (with a typical

amplitude of about 20°). Angle-dithering the crystal allowed for phase-matching at all wavelengths in the continuum, as schematically shown in Fig. (5.2).

5.2 SFG XFROG for SC probe characterization

A collinear type II SFG XFROG can be applied to the reference setup of Fig. 2.3 for the analysis of broadband continuum generation in photonic crystal fiber at the focal zone. Without taking off any optical piece of the reference setup, it is sufficient to add a SFG crystal at the microscope focus (which must be angle-dithered); a half-wave plate to each optical path before the microscope, and a monochromator immediately after it.

Here the use of the monochromator, instead of the spectrometer, is due to a different sampling mode. In fact, in the previous cases, the gate (or reference) pulse was mechanically delayed through a translation stage. Consequently, for each delay selection a vector 'FROG trace vs frequency' was collected. In this specific case, we are using a reference pulse which comes from the 1560 nm laser source and an unknown pulse that hails from the 780 nm source. As mentioned in Cap. 2 - Sec. 2.1, where the ASOPS technique is explained, the two laser sources produce train pulses characterized by different repetition-rates. In particular, the pump pulses have a repetition-rate $f_r = 100\,\mathrm{MHz}$, and the probe pulses repetition-rate differs from it of a small detuning value $f_r + \Delta f$. According to Eq. (2.2), for every pulse the probe beam collects a delay $\Delta t \approx \Delta f / f_r^2$ until to find itself again in coincidence with a pump pulse, after a time interval $1/\Delta f$. Therefore the FROG trace is automatically collected in function of the delay, without the installation of any delay line, and the delay resolution will just be Δt. For instance, choosing a detuning $\Delta f = 1\,\mathrm{KHz}$ we gets a delay resolution of $\Delta t = 0.1\,\mathrm{fs}$. On the other hand, the signal in frequency domain has to be resolved manually, by the use of a monochromator coupled with a photodiode. The combination of spectrometer and CCD camera can not be employed anymore because of the slow time response of the CCD camera. Therefore, in this geometry, for each frequency selection a vector 'FROG trace vs delay' is collected.

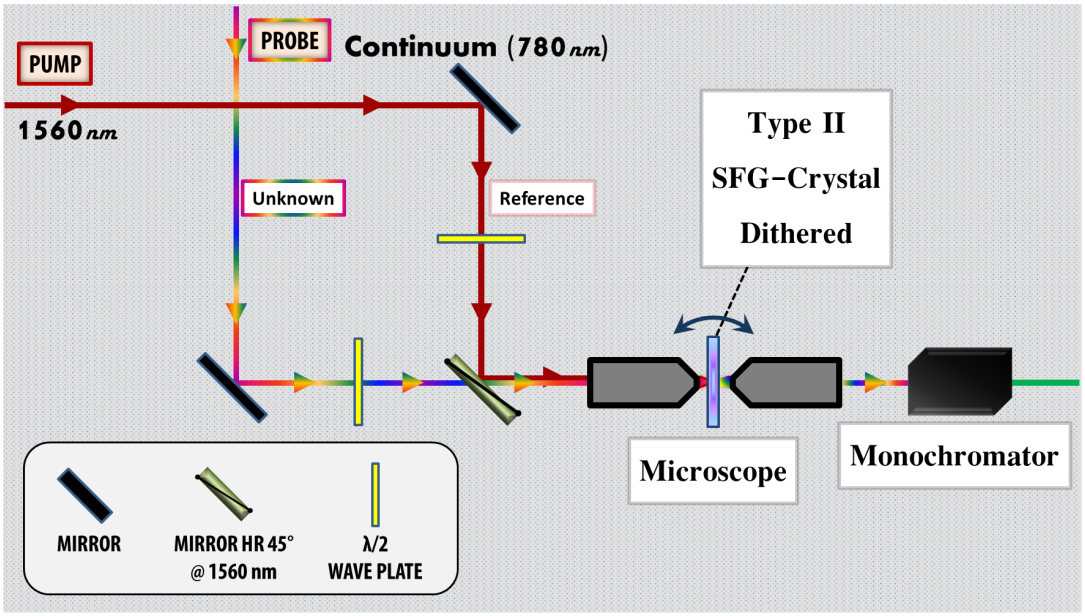

Figure 5.3: Type II SFG XFROG applied to our reference setup for the SC probe pulse characterization at the focus of the microscope objective. To work with this geometry the original probe laser (@ 780 nm) is used for broadband SC generation through a photonic-crystal fiber, which becomes our unknown pulse. The pump laser (@ 1560 nm) is exploited for the reference pulse generation. The optical line immediately before the microscope is modified introducing two half-wave plates. In this way the unknown pulse becomes an ordinary wave, while the reference pulse results in an extraordinary wave. The two pulses are made collinear and lead to the microscope. A SFG crystal must be placed in the focal zone, in the position where an hypothetical sample would be placed. Angle-dithering the crystal allows for phase-matching at all wavelengths in the continuum. Instead of the spectrometer, immediately after the microscope, a monochromator must be placed. Varying the wavelength selection of the monochromator the intensity in function of the frequency is measured; the intensity is already function of the delay since the ASOPS technique is involved (no delay lines must be added).

Chapter 6

Prospectives and conclusions

In this work we have firstly discussed two considerable multiphoton optical techniques, namely the pump & probe and the ASOPS techniques. Then, we have considered these methods to idealize a setup which involves monochromatic pump pulses and supercontinuum probe pulses. Since the setup was conceived to follow the thermomechanical dynamics of a nanostructurated sample, we have introduced an appropriate tailored microscopy system. Such a setup may become operative only through the characterization of both the pump and probe pulses at the foci of the microscope.

After a brief explanation about the temporal characterization, we have illustrated the FROG technique analyzing its experimental apparatus and phase-retrieval algorithm. To be thorough, we have reported the main FROG geometries with respective advantages and disadvantages.

Afterwards, we have shown how an appropriate collinear SHG FROG can be exploited for the characterization of the monochromatic pump pulses. To the purpose of testing the phase-retrieval algorithm, we have made some numerical simulation.

Later, we have discussed about the use of a collinear SFG XFROG for the characterization of the supercontinuum probe pulses. In our setup this method has the advantage of exploiting the ASOPS technique, so that the delay line can be avoided.

The FROG technique requires relatively common optical elements and it has the peculiarity to be low invasive in the experimental setup. Therefore, we are looking forward to apply it in a setup alike the idealized one.

Chapter 7

Acronimi

ASOPS *Asynchronous Optical Sampling*

BBO *Beta-Barium-Borate*

CCD *Charge-Coupled Device*

DFG *Difference-Frequency-Generation*

FROG *Frequency-Resolved Optical Gating*

FT *Fourier Transform*

IFT *Inverse Fourier Transform*

IR *Infrared*

KDP *Potassium-Dihydrogen-Phosphate*

$\lambda/2$ *Half-Wave Plate*

N.A. *Numerical Aperture*

PG *Polarization-Gate*

POL *Polarizer*

SC *Supercontinuum*

SD *Self-Diffraction*

SFG *Sum-Frequency-Generation*

SHG *Second-Harmonic-Generation*

STHG *Surface-Third-Harmonic-Generation*

TG *Transient-Grating*

THG *Third-Harmonic-Generation*

UV *Ultraviolet*

XFROG *Cross-Correlation Frequency-Resolved Optical Gating*

Acknowledgement

This thesis would not be possible without the help of many people. First of all, I would like to thank my assistant-supervisor Gabriele Ferrini, for proposing to me a topic which have fit perfectly the little time I have available and that, of course, I enjoyed a lot. Then I must thank the Trebino's group for having published the FROG code online. In particular my acknowledgements goes to Michelle Rhodes which came to the aid of me when I had problems with the program. Finally, I want to thank my parents for their encouragements and support.

Bibliography

[1] F. Medeghini, "Microscopia ottica risolta in tempo su singolo nanodisco", (2012)

[2] S. Peli, "Progetto e realizzazione di un apparato per spettroscopia ottica risolta in tempo mediante onda evanescente", (2010)

[3] C. Giannetti, B. Revaz, F. Banfi, M. Montagnese, G. Ferrini, F. Cilento, S. Maccalli, P. Vavassori, G. Oliviero, E. Bontempi, L. E. Depero, V. Metlushko, and F. Parmigiani,*Phys. Rev. B* **76**, 125413 (2007).

[4] Menlo System, *ASOPS white paper*, April 15 2009.

[5] A. Comin, C. Giannetti, G. Samoggia, P. Vavassori, D. Grando, P. Colombi, E. Bontempi, L. E. Depero, V. Metlushko, B. Ilic, and F. Parmigiani *Phys. Rev. Lett.* **97**, 217201 (2006).

[6] D. Nardi, M. Travagliati, M. E. Siemens, Q. Li, M. M. Murnane, H. C. Kapteyn, G. Ferrini, F. Parmigiani, and F. Banfi, *Nano Lett.* **11**, 4126 (2011).

[7] M. Travagliati, *Fabrication and time-resolved optical investigation of hypersonic phononic crystals*, Università Cattolica del Sacro Cuore, Master Thesis (2007); http://www.dmf.unicatt.it/elphos/.

[8] M. Travagliati, D. Nardi, F. Banfi, V. Piazza, and P. Pingue, *Thermomechanical decoupling in hypersonic phononic crystals*, MNE 2010 - 36th International conference on Micro & Nano Engineering: September 19-22, 2010, Genova (Italy).

[9] F. Banfi, V. Juvé, D. Nardi, S. Dal Conte, C. Giannetti, G. Ferrini, N. Del Fatti, and F. Vallée, *Appl. Phys. Lett.* **100**, 011902 (2012).

[10] V. Juvé, M. Scardamaglia, P. Maioli, A. Crut, S. Merabia, L. Joly, N. Del Fatti, and F. Vallée *Phys. Rev. B* **80**, 195406 (2009).

[11] G. V. Hartland, *Chem. Rev.* **111**, 3858 (2011).

[12] O. L. Muskens, N. Del Fatti, F. Vallée, *Nano. Lett.* 6, 552 (2006).

[13] R. Trebino, K.W. DeLong, D.N. Fittinghoff, J.N. Sweetser, M.A. Krumbügel, and B.A. Richman, D.J. Kane, "Measuring ultrashort laser pulses in the time-frequency domain using frequency-resolved optical gating", *American Institute of Physics*, (1997)

[14] R. Trebino, D.J. Kane, "Using phase retrieval to measure the intensity and phase of ultrashort pulses: frequency-resolved optical gating", *Optical Society of America*, (1993)

[15] K.W. DeLong, R. Trebino, "Improved ultrashort pulse-retrieval algorithm for frequency-resolved optical gating", *Optical Society of America*, (1994)

[16] K.W. DeLong, R. Trebino, D.J. Kane, "Comparison of ultrashort-pulse frequency-resolved-optical-gating traces for three common beam geometries", *Optical Society of America*, (1994)

[17] J.M. Dudley, X. Gu, L. Xu, M. Kimmel, E. Zeek, P. O'Shea, R. Trebino, S. Coen, R.S. Windeler, "Cross-correlation frequency resolved optical gating analysis of broadband continuum generation in photonic crystal fiber: simulations and experiments", *Optical Society of America*, (2002)

[18] Matlab FROG code of the Trebino group,"`http://frog.gatech.edu/code.html`"

[19] D. N. Fittinghoff, J. A. Squier, C. P. J. Barty, J. N. Sweetser, R. Trebino, M. Müller, "Collinear type II second-harmonic-generation frequency-resolved optical gating for use with high-numerical-aperture objectives", *Optical Society of America*, (1998)

[20] X. Gu, L. Xu, M. Kimmel, E. Zeek, P. O'Shea, A. P. Shreenath, R. Trebino, R. S. Windeler, "Frequency-resolved optical gating and single-shot spectral measurements reveal fine structure in microstructure-fiber continuum", *Optical Society of America*, (2000)

[21] P. O'Shea, M. Kimmel, X. Gu, R. Trebino, "Increased-bandwidth in ultrashort-pulse measurement using an angle-dithered nonlinear-optical crystal", *Optical Society of America*, (2000)